UNIVERSIDADE DA BEIRA INTERIOR
Engenharia

Feasibility of Applying Optical Sensors to Detect Fatigue Damage in Carbon Laminates

Liliana Patrícia Vieira de Freitas

Dissertação para obtenção do Grau de Mestre em
Engenharia Aeronáutica
(ciclo de estudos integrado)

Orientador: Prof. Doutor Abílio Manuel Pereira da Silva
Co-Orientador: Prof. Doutor José Miguel Almeida da Silva
Co-Orientador: Prof. Doutor Pedro Vieira Gamboa

Covilhã, outubro de 2014

À minha Avó

Ao Lucas

Acknowledgments

The elaboration of this dissertation and compliance with it would not have been achieved without the contribution of a few people, to whom I like to express my gratitude.

To Professor Dr. Abílio Manuel Pereira da Silva, my supervisor, for his unfailing and constant attention, support and encouragement which always kept me motivated throughout all the investigation.

To Professor Dr. José Miguel Almeida da Silva, my co-supervisor, for his suggestions and knowledge conveyed that was important for the realization of this work.

I am grateful to Professor António Espírito Santo for his important help in having provided the data acquisition system, which allowed me to get the intended results.

I also thank Mr. Paulo Guerra for the availability and knowledge transmitted to me, in the practice of fabrication of composite laminates.

I want to show my gratitude towards my neighbors for everything they have done for me. Thank you for the values you have instilled in me.

I want to thank my family for all the support they gave me and for believing in my abilities, when I doubted.

Last but not least, I want to leave a sincere thanks to my true friends, who accompanied me throughout my academic journey and always remained close.

Resumo

No setor aeronáutico, o menor defeito existente num material compósito pode comprometer a sua estrutura e reduzir significativamente o seu desempenho global.

A probabilidade de um objeto estranho embater numa estrutura da aeronave acontece desde o primeiro dia em que um elemento da estrutura passa pelo processo de cura e prolonga-se até o dia em que a aeronave é retirada de serviço.

A monitorização em tempo real, desde o processo de fabrico da estrutura e durante o seu funcionamento em serviço, quando esta é submetida a solicitações mecânicas, quer sejam estáticas ou dinâmicas, tem como objetivo otimizar o seu processo de fabrico, diminuindo assim as tensões residuais, e também é essencial na prevenção de danos catastróficos.

Tendo isto em mente, tem-se a intenção de verificar se o embebimento da fibra ótica no interior do laminado de carbono influencia o comportamento de fadiga, quando comparado com uma configuração semelhante mas sem a inserção do sensor (fibra ótica). Introduziu-se também, propositadamente, um defeito no plano médio do provete. Pretende-se verificar se o dano se propaga a partir do defeito, quando a estrutura é sujeita a carregamentos cíclicos.

Os laminados de carbono foram construídos com 18 camadas, com a fibra ótica e o defeito embebidos no plano médio do provete. Estes laminados foram testados à fadiga, através de flexão em três pontos e expostos a uma frequência de 10Hz.

Através dos resultados obtidos, observou-se uma diminuição no módulo de elasticidade e um aumento da temperatura, em ordem ao número de ciclos. Através da visualização dos resultados da emissão acústica, pode ser visto que existem alterações, sempre que existe uma variação na temperatura, tornando assim possível a utilização de um sensor óptico (com muitas vantagens) para a detecção de um nível crítico de avaria.

Palavras-chave

Compósitos, Estruturas aeronáuticas, Monitorização da saúde estrutural, Sensores de fibra ótica.

Abstract

For the applications in the aeronautics field, the smallest defect in a composite material can compromise the structure and significantly reduce their overall performance.

The probability of a foreign object hit an aircraft structure start on the day the first element is cured and will endure until the aircraft is retired from service.

The monitorization in real time from the manufacturing process of a structure, also during operation in service, when it is subjected to mechanical stresses whether static or dynamic, the optimization of the manufacturing process is made by decreasing the residual stresses. This monitoring prevents catastrophic damage.

Having this in mind, it was intended to verify that the embedment of the optical fiber within the carbon laminate influences the fatigue behavior, when compared to corresponding settings without embedding the sensor (optical fiber). It was also introduced purposely a defect in the middle plane of the specimen. It is intended to verify, when the structure is subjected to cyclic loading, if the damage is spread in the area where there is already the defect.

Carbon laminates were constructed with 18 layers, with the optical fiber and the defect embedded in the middle plan of the specimen. These laminates were tested for fatigue through three points and exposed to a 10Hz frequency.

By the results obtained, it was observed a decrease in the modulus of elasticity in order to the number of cycles. Meanwhile, there is an increase of temperature. Through visualization of the results of acoustic emission, could be seen that there are changes to whenever there is a variation in temperature thus making it possible to use an optical sensor (with many advantages) for detecting a critical damage.

Keywords

Composites, Aeronautical Structures, Structural Health Monitorization, Optical Fiber Sensors.

Contents

List of Figure

List of Tables

List of Acronyms

AE	Acoustic Emission
AFRC	Advanced Fiber Reinforced Composites
ASTM	American Society for Testing and Materials
CBM	Condition Based Maintenance
CFRP	Carbon Fiber Reinforced Polymer
FBG	Fiber Bragg Grating
FE	Finite Elements
FEM	Finite Element Method
FODDAS	Fiber Optic Damage Detection and Assessment Systems
FRP	Fiber Reinforced Polymer
NDE	Non Destructive Evaluation
OF	Optical Fiber
OFS	Optical Fiber Sensor
POF	Plastic Optical Fiber
SHM	Structural Health Monitoring
SMAs	Shape Memory Alloys
UAV	Unmanned Aerial Vehicle

Chapter 1 - Introduction

1.1 Motivation

Currently composites are increasingly been used in several areas of industrialization, as automotive, civil, aviation and marine constructions. The success is due to the advantages, over other kinds of materials, mainly because they present a low density, high strength and versatility due to the manufacturing process, making the structure simultaneously, strong and light [12].

The carbon fibers composites have many advantageous characteristics and their use is widespread. Lately a tremendous progress of the manufacturing process has been made, along with the improvement of resins, and their addition in appropriate proportions in order to obtain composite materials with better properties.

On the aeronautical industry, the smallest defect on a composite material can compromise the structure, and significantly reduce their overall performance [8]. The probability of a foreign object hit on an aircraft structure start on the day the first element is cured and will endure until the aircraft is retired from service [13].

Imagine a structure that has the ability to “feel” the influence of what is happening around her, as human being. This structure would be able to know its current status and, if necessary, put in place procedures to solve certain problems.

Monitoring in real time from the manufacturing process of a structure, but also during operation in service when it is subjected to mechanical stresses, whether static or dynamic, optimize the manufacturing process by decreasing the residual stresses. This monitoring prevents catastrophic damage.

The long-term behavior of composite structures can be predicted by numerical or experimental models. To ensure its integrity throughout its lifetime, it is necessary to do a thorough monitoring of its deterioration through an evaluation using nondestructive testing.

It is necessary to further study the behavior of smart composite materials, especially when damage isn’t visible. The impairment can be analyzed by an evaluation by embedding sensors in the material. Optical fiber is used as part of the sensor, due to its characteristics, such as: low weight, flexibility, high-speed transmission over long distances, low reactivity, electrical insulation, electromagnetic immunity and multiplexing of signals [14].

1.2 Objectives

With this work, it is intended to verify experimentally that the embedment of the optical fiber within the laminate influences the fatigue behavior when compared to corresponding settings without embedding the sensor.

In order to study the feasibility of monitoring structures, by inserting simple optical fibers as sensors, when they are subject to fatigue, the specimens were construed and tested.

1.3 Dissertation organization

The present thesis is divided in five chapters, in order to study the feasibility of applying optical sensors for carbon laminates subject to the fatigue.

In the first chapter, I will make an introduction, referencing work and previous studies performed by other authors, in order to give prominence to key topics for the elaboration of this dissertation.

The second chapter provides a literature review on the composites, more specifically carbon fiber reinforced polymer, optical fibers, optical fiber sensors and monitoring health structures.

In chapter 3, is described all the experimental procedure used in this work, the materials, and methods used in the elaboration of carbon laminates, that afterwards it will be mechanical tested.

In chapter 4, shows the results obtained for the experimental procedure, and the simulation done. A comparison between the two cases is made.

In the last chapter, chapter 5, it was presented the final conclusions and future works.

Chapter 2 - Literature review

Lately, in the area of structures and composites, materials have been studied and it has been analyzed the potential of smart structures for solving problems associated with the future development of structures. An example is the aircraft, with the ability to transform into full operation. These structures must be able to ensure their integrity, being able to respond to needs through actuators against potential critical situations as vibration attenuation.

The correct and efficient implementation of such systems requires the use of processors that allow for adaptation to the new conditions of the structure, through independent learning, based on the information provided by the sensors.

The sensors are devices that respond to physical and chemical stimuli that may be specific and measured analogously.

When inserting a sensor into the material, it has caused a defect in it, what conditioned the operation. The position in which the sensor was placed also affected the responsiveness, when subjected to external actions.

The use of composites in aircraft structures has been growing over the last few years. For instance, carbon fiber reinforced plastic (CFRP) composites have been used substantially for lightweight structures, as the airframe structures, due to the high specific strength and stiffness. CRFP have been replacing some metal alloys in several primary components in aircraft, since they improve the performance of these [1],[2], [16] .

Recently, research area of structures and composite material have studied and analyzed the potential of smart structures, on an effort to solve problems associated with the future development of structures. The aircraft is an example of a solution, with the ability to morph according to the operation. These structures must be able to ensure, not only the optimization needed, but also their integrity, being able to respond to needs through actuators against potential critical situations.

In order to make a correct and efficient implementation of such technology, it is necessary to devise a system, enabled to gather the information through sensors, embedded in the structure, complicate the data provided by the sensors, and process the information through previous collected knowledge. One of critical aspects of this technology is the effect in the structure [15].

When the fiber optic is embedded in material, it's created a discontinuity in the material, a careful study of the position, direction and thickness of the fiber optic fiber has to be taken, to ensure that the component is able to perform without compromising is viability. This is a matter that is widely studied in the literature.

A critical aspect of this appliance is the fatigue, the subject addressed in the effect is clearly measurable, the presence of the fiber optic limit the "life" of the component. Depending of the material, composites are optimized to work in just one direction, its important that the fiber has the same direction of the reinforced material [19], [21], [22].

Once fiber reinforced materials have a structural anisotropy and they contain different phases of material, fibers and matrix, result in various types of damage with different propagation characteristics [17].

The defects that are in composite materials can be difficult to detect visually, which implies maintenance and repair costs. The concept of self-healing can be an alternative to structures that have damage. This idea is based on the ability of living beings have to cure themselves, that is to avail the materials that are inside the structure to repair internal damage [8].

The inside structure of composite laminates can be monitored by non-destructive methods using optical fiber embedded in laminate structure. Introducing a foreign body, like an optical fiber within a structure, would be to create a defect and consequently endanger the mechanical performance of the structure.

2.1 Composites

A composite is characterized by being a combination of two or more materials whose junction has better properties than each individual material present. On these phases, different materials are generally used, with different properties and crystalline structure. From this definition one can find a wide range of materials that can be assumed as composite materials, as can be seen in the Figure 2.2 [18].

The materials that make a composite material can be categorized into two types: matrix and reinforcement, as seen in the Figure 2.1. The matrix material is what gives structure to the composite material, filling the empty spaces that remain between the reinforcement materials and keeping them in their relative position. The reinforcement materials are those which enhance the mechanical, electromagnetic or chemical properties of the composite as a whole.

The physical properties of a composite material depends on the geometric arrangement of the different phases of their respective volume fractions and also of structural factors such as the periodicity of each component. The geometric arrangement of the fibers (reinforcement) within the acceptor base material (matrix) continuous may be dispersed randomly nodes of a distributed or distributed irregular but repeating the repetitive and sequential manner (regular) shape.

Some of the features of the composite materials can be assumed to be additive, the final material having the properties of its components. However, this is not a rule; on the contrary, the resulting material shows related to the manufacturing process flaws such as spaces not filled by the material (eyes), zones of higher or lower frequency of the reinforcing material, resulting in an anisotropic material [19].

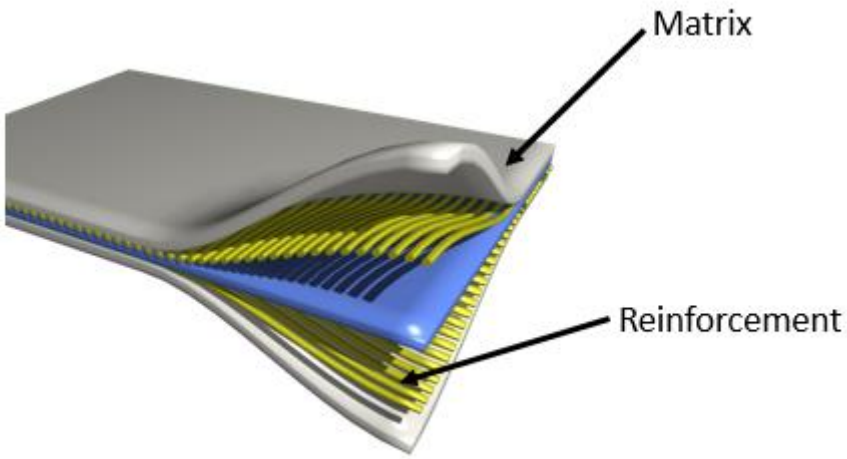

Figure 2.1 - Example of a composite material [1].

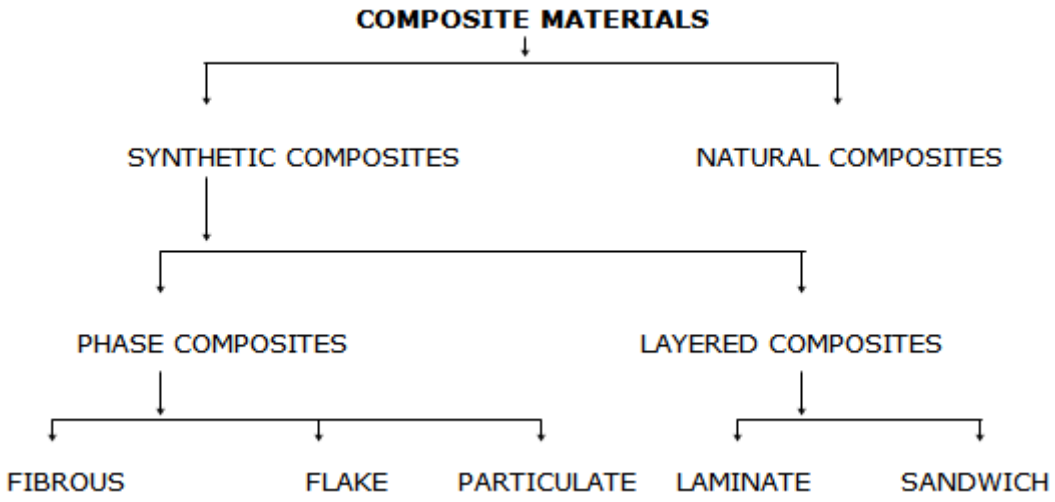

Figure 2.2 - Classification of composite materials [20].

To fulfill the objectives of this work was given emphasis on the synthetic composites. These are composed of mainly two phases: matrix and reinforcement. The materials for these phases are produced in separate being brought together only during the manufacturing process.

From this there is an important advantage of composite materials, which is the possibility of optimizing the final material, enabling the production of a material with properties impossible for any other kind of material by itself.

Composite materials are known to Man for a long time, however it was only in the early 30's that the so called modern composites appeared with the introduction of fiber glass. A Large-scale use of composite materials in the commercial industry was started by Airbus in its A300 vertical tail [2]. In Figure 2.3 can be visualized the percentage of total weight of composites used in commercial aircraft.

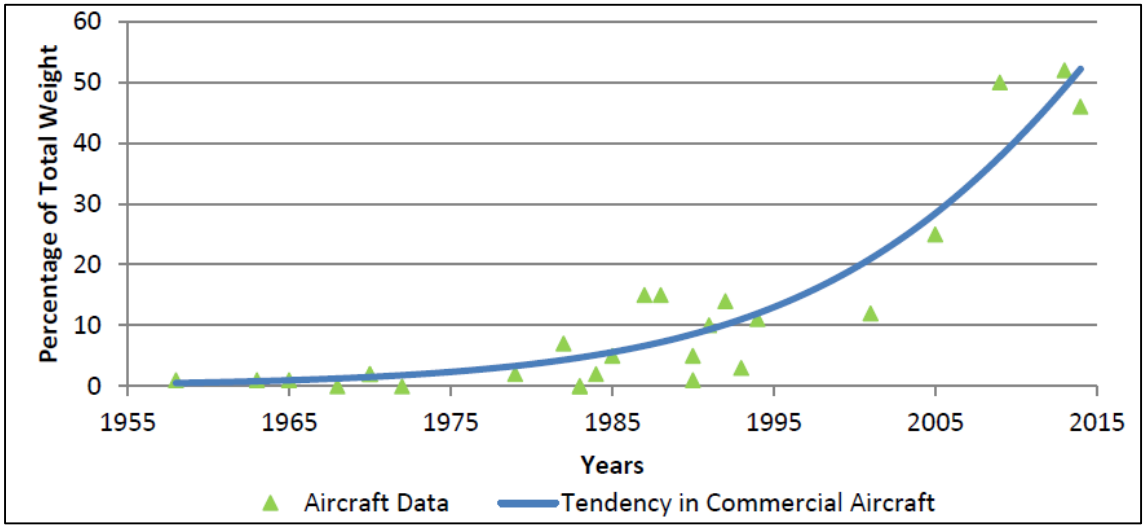

Figure 2.3 – Use of composite materials in commercial aircraft [2].

This type of material is used in space vehicles, aircraft, modern vehicles and light weight structure [21].

The use of composite materials in aircraft and aerospace industry is mainly due to these present clear mass reduction. Because they are low density materials allow a noticeable reduction in the overall mass to a similar degree in mechanical properties.

The first applications in the aeronautical industry were essentially in secondary structures such as fairings, small doors and control surfaces. After the Second War the expansion of air traffic forced aeronautical companies to fabricate aircraft able of transporting an increased number of passengers [2].

However, the employment of composite materials in the aeronautical industry was slower than expected. This was generally due to the high costs of certification and higher materials and production costs for composite components when compared to their metal equivalents [22].

Once the aircraft sector, the composite structures have thick parts that were intended to submit to high levels of structural loads. These loads can cause the nucleation and the growth of fatigue damage which can lead to structural failure. It is therefore important to understand the fatigue behavior of composite aircraft structures [23]. In Figure 2.4 can be seen the total materials and the percentage of composites used in Boeing 787.

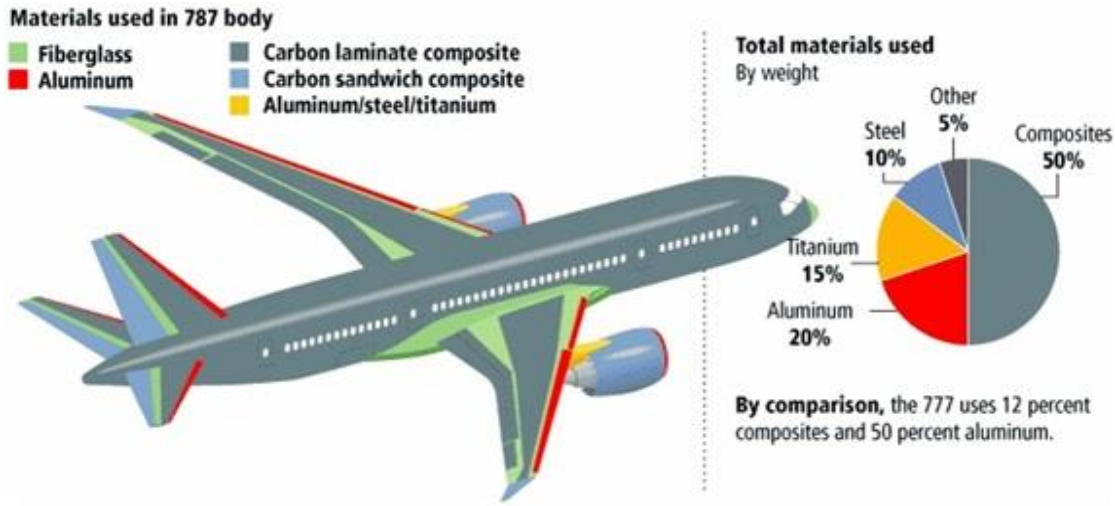

Figure 2.4 – The weight percentage of composites used in Boeing 787 [3].

2.1.1 Carbon fiber reinforced polymers

The CFRP laminates are very commonly used as structural materials because of their high specific strength and stiffness [24].

The Airbus A350F XWB is made up of the 53% of CFRP and the Boeing 787 Dreamliner is constituted by 50% of CFRP. Another application can be seen in the Figure 2.5.

The carbon-epoxy laminates are used in the aerospace industry due to their optimal ratio strength / density and stiffness / density. These are very commonly used, since it is intended

to maximize the cargo/passenger capacity, and overall efficiency, which are essential requirements in the design of aircraft [25], [26].

Figure 2.5 – A tail of a radio controlled helicopter, made of CFRP [4]**.**

When subjected to static or dynamic loads, laminates of CFRP presents damages, such as cracks and delamination. The appearance of delamination leads to a decrease in stiffness and could cause a catastrophic failure. For this reason, it is necessary to detect the failure before a catastrophic failure occurs [26], [15].

Composite materials, manufactured from resins and high strength fibers, also called advanced composites, are increasingly being used in structural components in aeronautical and aerospace industry. Epoxy resins are fragile and have poor impact resistance and tendency crack propagation, resulting in satisfactory levels of strength and reliability [27].

2.2 Smart structures

An inspection to a structure involves time and costs, even with the existing techniques (X-ray and ultrasonic C-scan). So there is a necessity to find techniques that allow to evaluate the worthiness of the structure, if possibly in real time. Therefore from the necessity, a solution was found, structures that use sensors in order to detect damage. This type of structures is known as smart structures [26],[21].

Smart structures have the ability to select and perform specific functions, in order to deal with stimuli or changes in the environment. Among its most promising features are: self-diagnosis, self-repair, self-learning and self-degradation [28].

The active elements in smart structures can be embedded into or attached in the structure.

Smart composite materials try to mimic natural structures, making the assessment of damage throughout the lifespan. With this type of composite materials, it is intended to provide

relevant data to engineers, such as: report a full history of the performance of the structure, location and dimensions and type of damage that may occur in the structure during his operation. According to this potentially dangerous or undesirable conditions can be prevented, giving an early indication for further test a repairs. These materials are able to act autonomously, due to external actions that might be subjected.

Currently the objective of several researchers aims to develop materials and structures that with the ability of self-motorization, will allow that material/structure actively adapts to the surrounding environment.

A smart materials system is composed of sensors and actuators. The actuators have a similar function to the muscles, and sensors have a similar architecture to the nerves, which allows the communication network to the central unit of the control system [29].

The first applications of smart materials and structural concepts will be on rotorcraft blades, aircraft wings, air inlets, engine nozzles, large deployable precision space systems and robust microspacecraft [30]. An example of the application of smart structures is show in Figure 2.6.

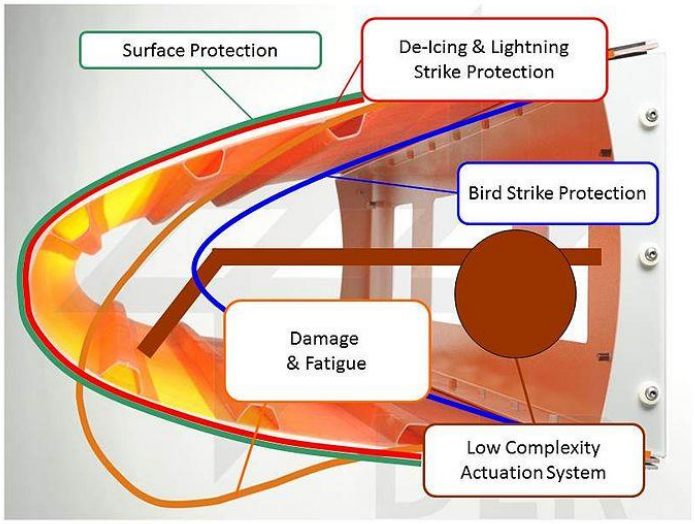

Figure 2.6 - Example of a smart structure. This structure consists of a flexible outer skin and an internal driving mechanism [5].

2.3 Optical fibers

It is necessary to further study the behavior of smart composite materials, especially when the damage is not visible, due to the size material or form of the structure. This damage can be analyzed by an evaluation obtained by the introduction of optical material.

An optical fiber (OF) is a waveguide which presents a diameter in the order of 0.1mm that has the ability to conveying light upon kilometer range distances [31].

The OF can be selected to suit specified end-use applications and operating temperatures. A conventional OF consists of two basic components, a core and a cladding. The core has a higher refractive index than the cladding and light is propagated along the core through total intern reflection. It is applied to the outer fiber, a protective coating (polyacrylate or polyimide), to provide mechanical and chemical protection [32]. Light is guided in the core of the optical fiber via total internal reflection, see Figure 2.7.

OF can be used to monitor a wide range of parameters including strain, temperature, pressure, humidity, vibration, specified chemicals (ageing or degradation), acoustic emission and fracture [33],[34].

Optical fibers are electromagnetic interference proof, and therefore can be used in areas where electrical-based devices cannot operate without expensive shielding and protection.

Recent advances in analytical instrumentation and OF sensor systems, made possible to obtain in-situ cure kinetic data during the processing of reinforced plastics. Optical fiber-based sensors are also used to enable real time structural health monitoring of engineering composites and structures [15].

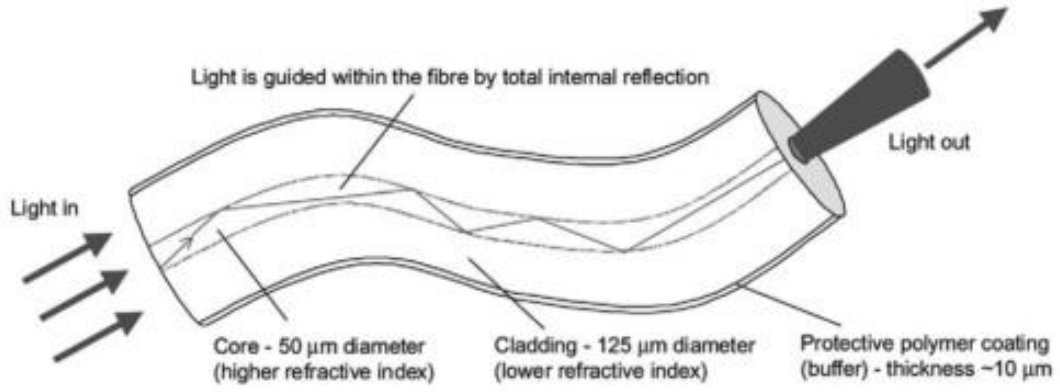

Figure 2.7 - Schematic illustration of an optical fiber [15].

The relatively small dimension and uniform cross-section of the OF, make it easy for surface rising or embedding. When embedded, they tend not to influence the quasi static tensile mechanical properties. However, when the optical fiber sensors (OFS) are embedded off-axis, this is not the case, the compressive properties may be affected.

2.3.1 Optical fiber sensors (OFS)

The use of optical fiber in sensors applications is growing, driven by the large research done in this area in recent years, and taking the advantages of the optical technology when compared with the electronic solutions [20].

A sensor is a technological device that detects signal by means of the change of a specific or general parameter. Thickness, is also important, the interference is minored, when the optic fiber, and the reinforce fiber have the same magnitude of dimension. If that is no taken in account, it´s normal to see the appearance of defects, like delamination of the material around the optic fiber. Other important parameters are the stiffness, strength, and Poisson ratio, of the material, in literature [23], the effect of the presence of the fiber is very small in this parameters. They can be applied to collect information such as strain [18], [24], [25], [26], vibration (frequency, displacement) [27], buckling [28], fatigue [17], damage detection [29], [31], [32], [30] and terminal variations [33].

OFS use all the optic fiber embedded on the material "to gather" the information, but there are key differences in the sensors. It's not possible to use the same sensor to collect a wide spectrum of information. So to collect dense spectrum of information it is needed to use also many different sensors, optimized to collect a single kind of information.

The OFS offers many advantages when compared to traditional electronic sensors. It is light, small and immune to electromagnetic interference, not subject to metallic corrosion, can be deployed in areas where electrical-based sensors would fail, or require expensive protection. They can also be deployed in harsh chemical environments, with an appropriate sensor protection system [31]. They can be directly embedded within materials as in the case in advanced composites in order to provide sensing networks for the damage detection or health monitoring of smart structures [35], [36], [37].

Fiber optic strain sensors have been applied to internal strain and damage monitoring of composites because of its small size, light weight and flexibility. Optical fibers can be integrated directly and easily into fabrics [30].

OFS can be multiplexed. With certain sensor design, distributed sensing can also be achieved along the length of a fiber. These characteristics are very attractive, for process monitoring, because parameters such as the chemical composition of specified functional groups and temperature can be obtained in real-time from the processing equipment [15].

FOS systems can provide real-time and in-situ data on the chemical and structural integrity of engineering materials and structures. These devices can be engineered to have minimal adverse effects of the host materials. It is capable of measuring static and dynamic strains when embedded or bonded on a structural component [38].

Sensors embedded in the fibers of the composite material enables a high sensitivity in the determination of damage to the material because of its small dimensions.

The optical fiber sensor can be ideal for integration with composites, since it is manufactured, it allows the optical fibers to become embedded in the composite without necessarily affecting its macroscopic properties.

The biggest advantage of this type of sensors is its ability to check the "health" of various components, during their period of service. The basic functions can be divided into three main areas, which are: detection of environmental conditions around the structure; transmission of information gathered for a central processing unit and signal processing and performance of functions in response to stimuli senses.

In Aerospace application, the development of smart structures with integrated optical fibers relate to space systems such as satellites, launch vehicles or even seasons. For example, the detection of leaks from tanks propellants is now a reality. Currently, the solution appears to be the use of an optical fiber network, built these tanks during the manufacture by rolling prepreg material. Another application is the possibility of using a smart composite coating that can detect their impacts and thus damage the surface of satellites or space stations.

The mechanical characteristics of composite laminates with the embedded OFS were evaluate by Lee, Lee, & Yun, (1995) [39]. They investigated the effect of embedded optical fiber on the mechanical properties of composite laminates subjected to static tensile and low cycle fatigue load. The embedded OF doesn't have significant effects on stiffness, strength and Poisson's ratio under the static tensile load.

S. Minakuchi and N. Takeda [6] mentioned in their work that when optical fiber sensors are embedded into composite materials during the manufacturing, the sensor can be used to continuously, monitoring the manufacturing process itself, in-service usage and damage. By combining all the information obtained by the distributed sensing network, they prove that it possible accurately evaluate the structural health [5]. This can be seen in Figure 2.8.

Fiber optic distributed sensing schemes have been studied to make smart structures and materials. These sensors systems, which are known as "fiber optic nerve systems", senses damage induced in materials and structures, in which the fiber is embedded [34].

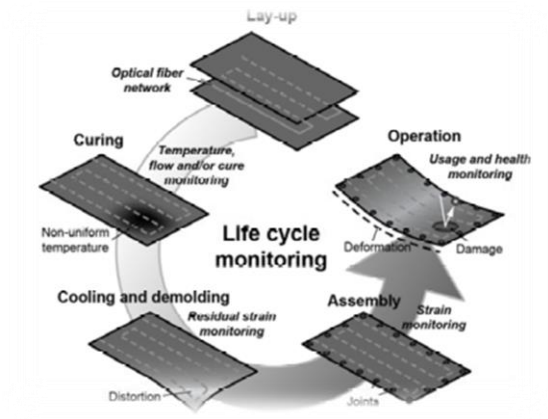

Figure 2.8 - Illustration of life cycle monitoring [6].

2.3.2 Optical fiber sensors for damage detection

The damage tolerance and durability of composite repairs are currently substantiated by the analytical, numerical and experimental studies, and by comparison with existing composite repairs [40].

For many structures, failure is preceded by the formation and propagation of cracks. An important challenge in crack monitoring is that the location of cracks in structures may not be known in advance. Conventional sensors or transducers that measure the average strain over a small region may easily don't sense the crack [41].

OFS have been prominent in health monitoring of aerospace composite structures. On the application of composite structures, the reliability and safety shouldn't be dismissed. The implemetation of sensors to detect the damage will provide reliable results about the state of the structure [6].

In real structural applications, the strains applied to the composite structures are difficult to predict; therefore real time strain monitoring is needed to foretell the present damage status in composite based on above durability evaluation method [42], [43].

The methods currently used to detect damage demand the structure to be taken out of service, and often disassembled which is both uneconomical and difficult to implement. Thence fiber optic sensors can be embedded into a structure and supply real time in situ measurements of condition, making it a promising alternative to other methods of damage detection [21].

Takeda (2002) [43], applied two kind of embedded optical fiber sensors, plastic optical fibers (POF) and fiber Bragg grating (FBG), to detect and monitor the transverse crack evaluation method.

Other application of this kind of sensors has been developed by Murayama, Wada, & Igawa, (2013) [44]. They developed a fiber-optic distributed sensors to be implemented to the damage detection of a single-lap joint and load identification of a beam simply supported. It was prove that by applying the distributed sensor to SHM it could be improved as making the spatial resolution higher and they have shown that the simulation technique taking into account both the structural and optical effects seamlessly in strain measurement could be a powerful tool to assess the performance of a system for detecting and design it for SHM. See Figure 2.9.

A smart structure system based on fiber optic vibration sensors has been developed by Leng & Asundi, (2002) [45], to monitor structural damage. The FOS has been embedded in the carbon/epoxy composite specimens and surface mounted on the surface of aluminum specimens. Tests were performed to examine the various types of damage to these specimens. The results showed that such kind of multimode fiber optic sensor can be used in the non-destructive evaluation of smart material.

Another application is FODDAS (fiber optic damage detection and assessment systems) which are built in laminated composite structures and are based on fiber optic strain sensors or sensor networks, providing multiple strain measurements. Leng & Asundi (2002) [45] made a review about these systems. These fiber optic strain sensors and sensor networks have been developed to the point where it can become the enabling technology in the development of such systems. The principal objective of this technology is detection of damage, the location's determination of the loading/damage sites and the quantitative evaluation of severity of the damage.

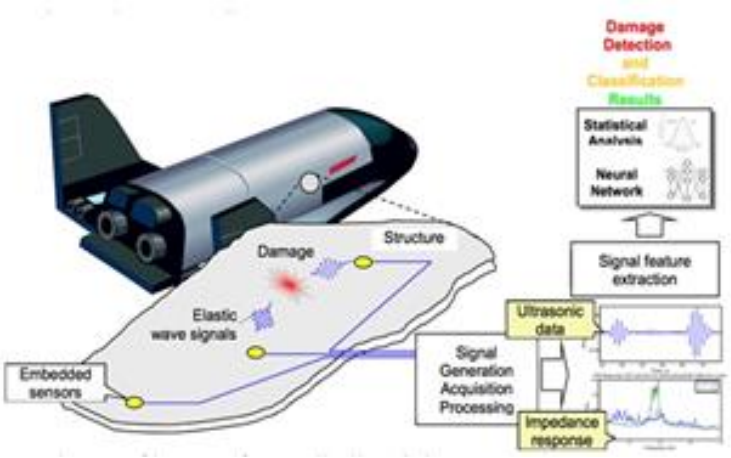

Figure 2.9 – The idea of the spacecraft SHM system [7].

2.3.3 The influence of the optical fiber embedded

By inserting optical fibers in the materials, in ideal conditions should be kept in account the properties of the optical fiber, and the material which will be embedded and still take into consideration the conditions of the embedding process [33].

The diameter of optical fiber is larger than the diameter of reinforcement fiber, as a result of the presence of embedded optical fibers on the mechanical properties of host material is necessary. Study and analyze is important [35].

The best orientation for the fiber, will cause slightest disturbance is parallel to adjacent reinforcing fibers. Inappropriate OF properties for the intended embedding application may lead to early fiber failure. A damaged optical fiber can still be used as a sensor, if the signal is interrupted [13].

The incorporation process for the inclusion of the optical fiber, may require that the embedded fibers and lead, and part of it led to fiber lengths withstand high temperatures that can melt the coating of the material or otherwise lose its effectiveness as a protective layer. Not long ago, coatings of higher temperature polymers such as polyimides, have been developed, that allow the processing temperatures required for manufacturing composites, and other low temperature materials, but that in turn fail at even higher temperatures [33].

Benchekchou & Ferguson, (1998) [46] applied Finite Elements (FE) techniques to simulate the strain and stress concentrations in and around an OF embedded in carbon fiber reinforced laminates. Analytical results show the location of high stresses and therefore the position of possible damage when specimens are subjected to tension and flexure. Mechanical fatigue tests are carried out on specimens with optical fibers embedded within different orientation plies, in order to see the effect of the fibers on the fatigue behavior of the specimens. 3D FE simulations have shown that the presence of an OF within a carbon fiber specimen, while it's subjected to flexure and tension, doesn't significantly change the stress distributions in plies other than those where the OF is embedded [46].

Loutas, Panopoulou, Roulias, & Kostopoulos, (2012) [47] showed through their work of SHM that the location of the OF in a specimen is important, once could modify theirs fatigue behavior and its resistance [47].

By embedding in composites, under the static tension and cyclic fatigue load, it is know that the embedded OF doesn't significantly alter the stiffness, strength and Poisson's ratio under the static tensile load. On the other hand, under the fatigue loading, significant reduction of fatigue life of composite structure with embedded OF was noted. Especially, embedded OFS shows very low fatigue resistance in the cross ply laminates. Matrix crack density of cross ply laminate was not affected significantly by embedded OFS under both the static tension and the cyclic fatigue loads [39].

Silva, José M. A. et al (2005), [49] performed three kinds of mechanical tests: impact tests, static flexural tests and fatigue tests. The results for the mechanical behavior in static loading conditions seems to be not significantly hampered as a consequence of the presence of the OF. In the case of impact and fatigue tests, these are strongly affected, despite this influence is physically different from each other [49].

In the frame of a numerical/experimental study on the monitoring of the skin buckling phenomenon in stiffened composite panels by embedding OF, a numerical procedure, for the design of OF embedding, has been introduced by Riccio, A et al (2012) [22]. This procedure demonstrated to be able to provide the most efficient embedded OF path (with minimum length) satisfying the grating sensors locations and directions requirements and fulfilling specific embedding/integrity constraints for the optical fiber [22].

Huang, C. Y. et al (2010) [8] made a study about the influence of embedded circular hollow vascules on structural performance of a fiber reinforced polymer (FRP) composite laminate. By incorporating these vascules, they have multifunctional composites, whose characteristics are self-healing and active thermal management. On the other hand, the presence of off-axis vascules leads to localized disruption to the fiber architecture, for instance, resin rich pockets, which are considered as internal defects and may cause stress concentrations within the structure. This can be visualized in Figure 2.10. It has been developed a manufacturing method for forming vascules, microscopic characterization of their effect on the laminate, finite element analysis (FEA) of a crack initiation and failure under load and validation of the finite element via mechanical testing observed using high-speed photography (HSP) [8].

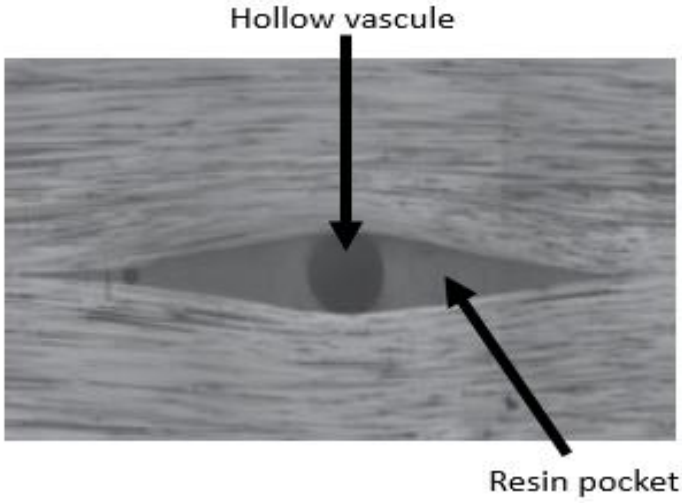

Figure 2.10 – Cross-sectional optical micrographs of circular vascules forming a resin-rich pocket in a CFRP laminate [8].

2.4 Structural health monitoring (SHM)

Structural reliability and operational health monitoring have become more and more important in most aerospace and civil engineering applications over the past decades, where the philosophy of fail-safe has prevailed about the safe life approaches in the design of metal structures and composite [50], [51].

In order to allow the increase in the use of composite materials in the aeronautical industry one must be able to certify and validate the components making use of these materials. For that, the technological capability of inspecting those components for defects and flaws, after production or during the component's life cycle, is paramount.

The flaws or defects, in what composite materials is concerned, very often occur inside the material, therefore being impossible to identify without breaking the component, so, non-destructive inspection methods are employed. Most conventional non destructive evaluation (NDE) techniques such as ultrasonic C-scan, x-ray, thermography and eddy current are limited as they require structural components of complex geometry to be taken out of service for a substantial length of time for post-damage inspection and assessment [52].

SHM can be viewed as the integration of sensing and intelligence to enable the structure loading and damage, which in turn causes conditions to be recorded, analyzed, localized and predicted in such a way that nondestructive testing becomes an integral part of them. The difference between conventional NDE and SHM it is that SHM uses sensors that are permanently attached or built into the structure and NDE don't use [9].

SHM have a purpose, which it is to lead a structure to be safer at the lower cost [44][53].

Composites, which are highly susceptible to occult internal failures that may take place during the manufacture and processing of the material or structure when it is submitted to service loads, demand a substantial quantity of defects monitoring and inspection at regular intervals. In Figure 2.11 it can be seen the keys parts of a typical aircraft to be monitored.

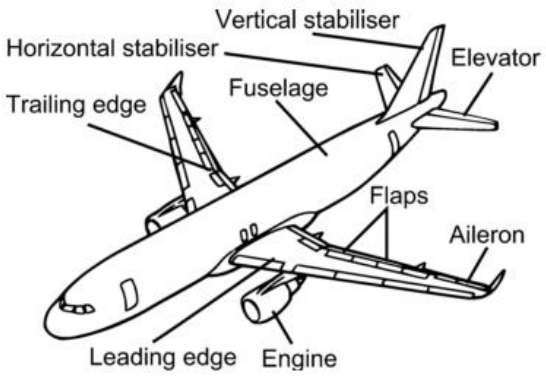

Figure 2.11 – Illustration of keys parts of a typical aircraft to be monitored [9].

With the technology of sensing, a reduction in cost, size and weight, and output processing of the sensor signal continually growing, wide potential approaches were developed, allowing the integration of such detection options on or inside structural components [54].

The actual reduction of life cycle costs associated to maintenance and inspection can only be reached by SHM "fail-safe" systems designed and included as components within an environment evaluation of the damage tolerance, capable of reducing inspection times, making the assessment to structure rapid and reliable, and avoid time consuming disassembly of structural components.

Optical fiber sensors have attracted considerable attention in health monitoring of aerospace composite structures. Benefiting from its advantages, OFS promise to be an alternative sensing techniques in SHM systems and upcoming smart structures [27], [55].

The main reason why it's important monitoring structural integrity is the ability to observe the in-situ structural behavior under different load conditions for a predetermined time or throughout the service life of the structures. Through this observation, the deterioration of material properties and/or structural response can be determined when it is subject to certain conditions of solicitation.

Murayama, Wada, & Igawa, (2013) [44] have reviewed researches about SHM with the fiber optic distributed strain sensor. Loutas, Panopoulou, Roulias, & Kostopoulos (2011) [50] developed a new system for structural health monitoring of composite aerospace structures based on real time dynamic measurements, in order to identify the structural state condition. Long-gauge Fiber Bragg Grating (FBG) optical sensors were used for monitoring the dynamic response of the composite structure[44], [50].

Damage detection, life cycle monitoring and shape reconstruction systems applicable to large-scale composite structures have been studied and described by Minakuchi and Takeda (2013) [6]. They highlight the potential of OFS for the SHM field [6]. See Figure 2.8.

Loutas, Panopoulou, Roulias, & Kostopoulos (2012) [47], create an intelligent system for structural health monitoring of aerospace structures, based on dynamic strain measurements. They used FBG's optical sensors for collecting data, representing the dynamic response of the structure. The main purpose was identified in an exhaustive way the structural state condition[47].

Data processing obtained from an airborne, load tracking and structural health monitoring system were presented by Kressel, I. (2013) [56]. The system is based on optical Fiber Bragg

sensors embedded in the two tail booms of an unmanned aerial vehicle (UAV). Flight data were analyzed both in the frequency and time domains, so that abnormal structural behavior could be identified and tracked, and its impact on structural integrity evaluated. Tracking the structural behavior over time can be used for Condition Based Maintenance (CBM), and may eventually reduce maintenance cost and aircraft down-time [56].

A SHM system can be seen as a kind of imitation of the human nervous system with built-in sensor and diagnostic capabilities, as shown in Figure 2.12.

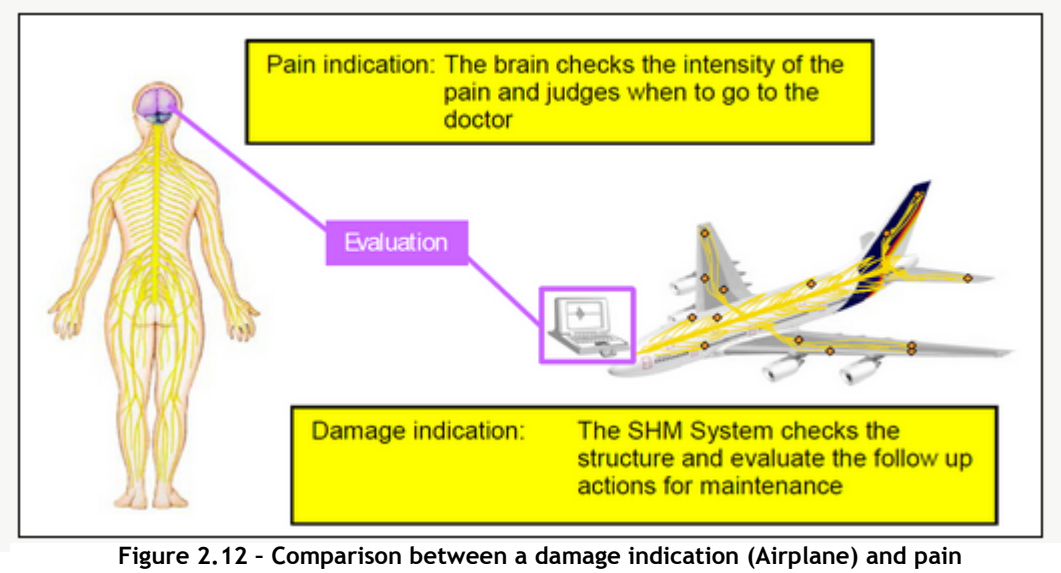

Figure 2.12 – Comparison between a damage indication (Airplane) and pain indication (Human Being) [57].

Chapter 3- Experimental procedure

To accomplish the goals of this study, carbon laminates were constructed and characterized. In this chapter, the techniques used in the manufacture of the test specimens, from preparation until they are cured in an autoclave and the test to which they were subjected, in order to get the results of the required parameters, have been described.

It was addressed the techniques used to obtain the parameters of temperature, intensity, acoustic emission and modulus of elasticity, which result from the trials that the specimens were subjected.

The manufacture of the test's specimens cure them and the trials to which they were subject, have been made according to norms.

Finally, it was mentioned the main problems throughout the experimental procedure.

3.1 Materials and methods

In the manufacture of the specimens were used the pre-impregnated carbon material with epoxy resin, Texipreg HS 160 REM, that can be seen in the table 3.1 (Annex A), Polytetrafluoroethylene (PTFE) for the defect and the optical fiber used is F-MLD 100 μm from Newport (Annex B).

The optical fiber used can be divided in three main parts, as it can be seen in the Figure 3.1. The part (1) is the core (100±4 μm diameter) and it's made by glass. The other parts are made with silicone and are named cladding (140±3 μm diameter), (2) and coating (250±15 μm diameter), (3).

Table 3.1 - The basic properties of Prepreg material[11].

Typical Prepreg Properties	Unit	Typical values
Outlife @ 23ºC	days	30
Storage life @ -18ºC	Months	12
Cured resin density	g/cc	1.2
Tg fully cured	ºC	130
Gel time @ 125ºC	min	12'00±3'00

The carbon laminates have a rectangular shape 150x40 [mm^2] and a nominal 2.5mm thickness resulting from a total of 18 plies stacked in [$90_20_290_20_290_1\ OF\ 90_10_290_20_290_2$] configuration.

The defect has a rectangular shape 40X10 [mm^2] and the optical fiber is located in the transversal direction.

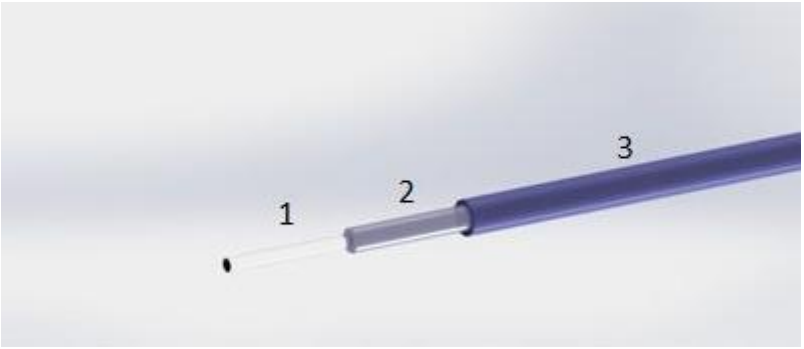

Figure 3.1 – Illustration of the optical fiber used in the work.1-Core; 2-Cladding; 3-Coating.

Simple test specimens were also constructed, in other words without the insertion of the OF and the defect. These have been set for the purpose of subject them to bending tests on 3 points. With the obtained results, for simple test specimens and for test specimens with fiber optics and embedded defect, the ultimate strength value was calculated.

After mounting the carbon laminates, with the optical fiber and the defect in the middle plan, as illustrated in Figure 3.2, they were placed in the autoclav**e.**

The autoclave, is a pressure vessel where the consolidation of the stacked prepreg is achieved by the application of a vacuum, through a vacuum bag and external pressure. Curing is obtained by the application of heat. Here, there will be a cure of the laminates with temperature and pressure maximum values of 125ºC and 7 atm, respectively, in order to give the best material properties and the lowest dispersion between different specimens.

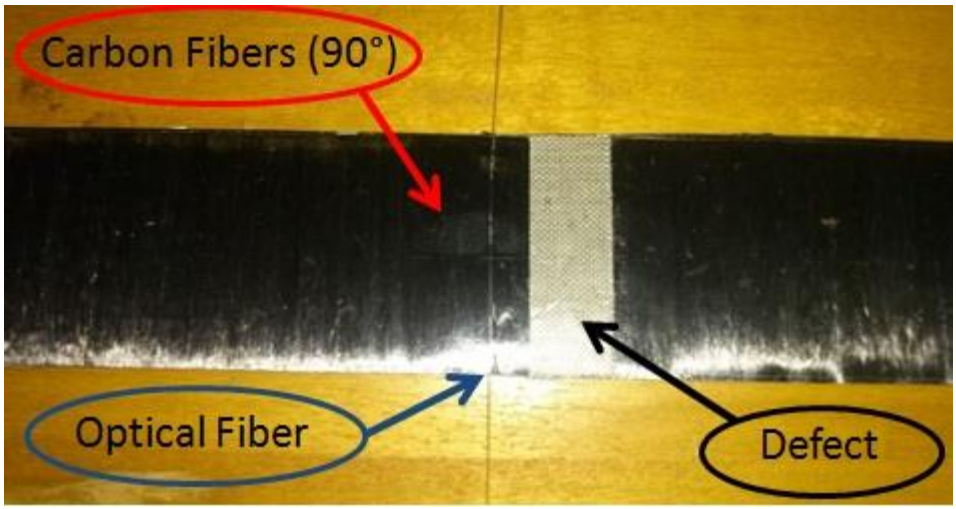

Figure 3.2 - Illustration of the layout and location of the optical fiber and the defect.

After the stacking of all laminate, and inserting the optical fiber and the defect, a bag was built for test specimens could be placed in the autoclave. The bag is constituted by a tape of named heat-resistant plastic film by vacuum and the end is closed by a sealing machine for heat fusion, leaving only a connection between the inside and the outside of the bag through a valve where is connected to an air pump to create a vacuum in the bag.

In Figure 3.3, it is shown the arrangement of samples. This image does not picture the geometry of the specimens used in this work. But the arrangement of the laminates is the same. As the Figure 3.3 shows, three test pieces was placed each time, to avoid damaging the optical fiber, since this exceeds the geometry of the specimen. It is important to protect the optical fiber, to avoid contact with the waste resin during the cure.

To protect the optical fiber, it was rolled up and placed between two Teflon papers and also placed near the specimen, bostik, in the area where the optical fiber came out. In the construction of the bag it was important to protect the optical fiber, so after autoclave curing, so when the samples are remove, the OF can be intact. Its integrity was important for the whole experimental process, since it gives the optical signal and hence through its analysis, it is seen whether it can operate as sensor.

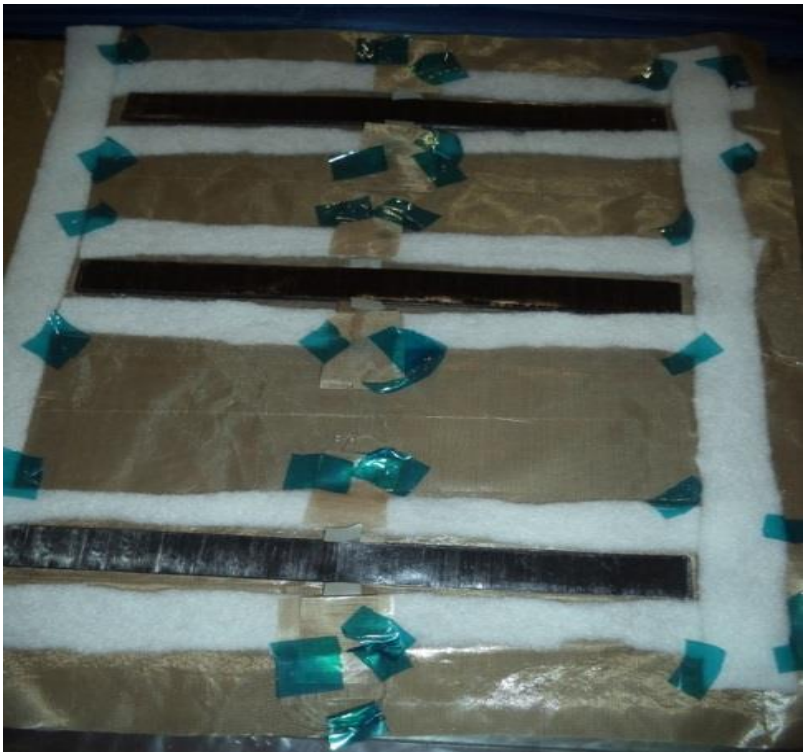

Figure 3.3 – Preparation of the bag to take the laminates to the autoclave.

During the healing process, it is necessary to comply with the conditions that the manufacturer recommends for prepreg materials in an autoclave [11].

In the end of the curing process, the specimens were removed from the bag, very carefully so that it the optical fibers were not damaged.

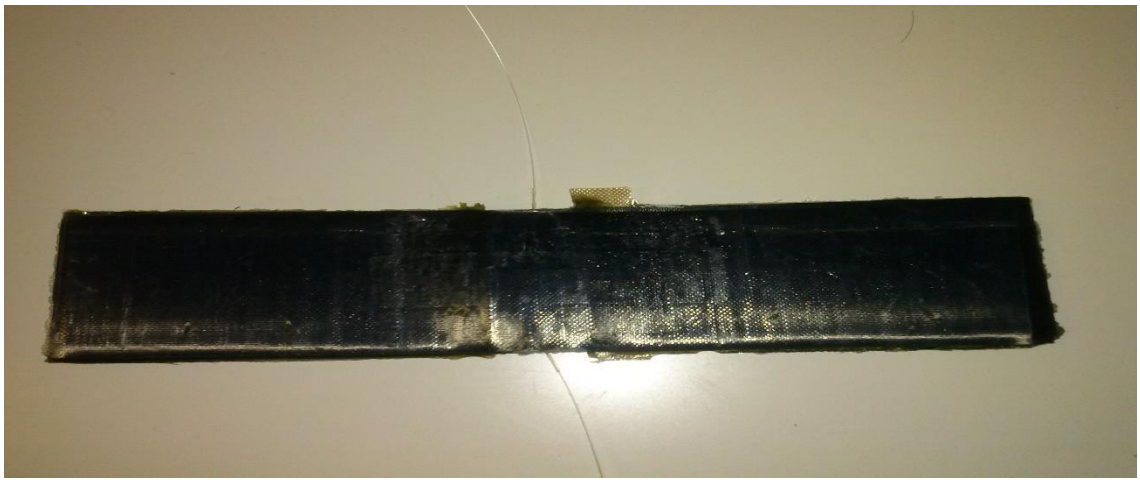

Figure 3.4 – The aspect of the specimen with the O.F. and the defect, after the process of autoclave curing.

To achieve a better optical signal, and consequently better results, the optical fibers were submitted to a treatment, in which the coating was removed at their ends after being dissolved in acetone. The extremities of the optical fibers were cleaved so that it obtains a maximum light signal.

One extremity of the optical fiber receives the signal from a laser, Melles Griot brand, see Figure 3.5, having a maximum power of 10mW, while the other extremity is inserted into a light sensor Newport-818 DO-M, and optical power player, of Newport, model 835, which indicates the instantaneous signal power bright. To make this procedure is used the device of the Figure 3.5.

Figure 3.5 - Laser used for the production of the light signal.

In the output of this device is connected a data acquisition system, developed by Professor António Espírito Santo, which allows the acquisition of light sensor values through the Matlab program (Annex C).

The values of the room temperature and of the specimen temperature were measured by a thermocouple attached to the surface of the specimen. To obtain these temperature values, a code in Matlab was created, which can be visualized in Figure 3.6.

Figure 3.6 – Illustration of the equipment which were made the acquisition of ligth sensor values.

Figure 3.7 – Equipment used for the acoustic emission tests.

Some acoustic emission (AE) tests were made using a Marandy MR 1004 equipment, see Figure 3.7 connected with a broad range piezoelectric transducer, which was attached to appropriate software so that to acquire the total countdown of all events detected.

It is possible to use this test to distinguish between different damage mechanisms acting during cyclic loading. It was possible to detect distinct AE levels.

3.2 Aging of the test specimens

Five specimens were subjected to sixty thermal cycles, and other five specimens to thirty thermal cycles. Each thermal cycle varies between -25 degrees and 80 degrees and has duration of 1 hour.

These values were chosen to represent the more realistic conditions that may occur during flight envelope. In order to simulate the negative temperature values, specimens were placed in a freezer. The stove was used in case of high values of temperature.

After performing all the thermal cycles, the values of temperature and variation of elastic modulus for specimens with sixty and thirty temperature cycles, were compared. It was also compared these results to those obtained for specimens without thermal cycles.

3.3 Static three-point flexural tests

The specimens with the optical fiber and defect and simple specimens, were subjected to static three-point flexural tests. Through the analysis of the results of both types of specimens, was found the ultimate strength value. It is important to find this value, before performing the fatigue tests since it is essential to characterize samples.

The static three-point flexural tests were performed, in accordance with the norm D790 ASTM (Annex D), using an Instron 1341 with wavematrix control software. See Figure 3.8

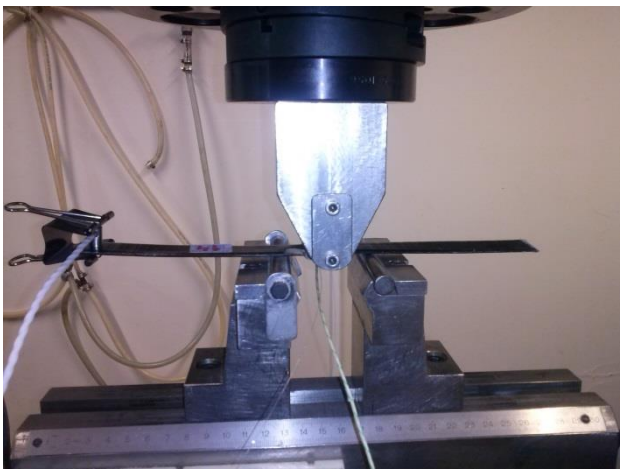

Figure 3.8 – The testing machine Instron.

3.4 Three-point bending fatigue tests

Fatigue tests were performed on an Instron 1341, controlled by software, Instron 8800 Fast Track, which makes the acquisition results of the force applied and the resultant strain present in the specimen.

Through the analysis of Figure 4.1 and 4.2 for the ultimate strength value to the simple specimens and the samples with optical fiber and defect embedded, it was decided to use 70% of the ultimate strength value.

Regarding the choice of frequency, after performing tests for 6, 10 and 20 Hz and analyze their results compared to the variation of temperature and Young's modulus, it has been selected the frequency of 10 Hz to carry out the testing.

From Figures 4.3 and 4.4 it was concluded that the value 6Hz not cause large changes in temperature. This causes the frequencies of 6 and 20 Hz cannot be used in this test since that is intended to there are significant temperature changes and so consequently, the optical signal will be able to detect possible damages in material.

A stress ratio of 0,1 was used and a time constraint was imposed of 500000 load cycles.

The data acquisition software is activated by a signal (step) output by the Instron system starts precisely when the bending test, thus synchronous obtained results, force, power and distortion of the light signal.

The tests performed are made with spacing between supports of 50 mm and a crosshead speed of 2 mm / min.

Each test specimens was tested individually. Therefore the entire experimental procedure was repeated for each sample.

3.5 Difficulties

During the testing procedure some shortcomings resulting in the extension of the experimental work appeared.

One major difficulty was the protection of the optical fiber, when it was placed in a vacuum bag and put in the autoclave. The major difficulty was to minimize or avoid contact of the optical fiber with resin waste, when the specimens were in the autoclave. When removing specimens of the vacuum bag, it is necessary to carefully handle specimens, and remove the

protection that had been done to the optical fibers. This step has proved itself particularly difficult, and in some occasions was unsuccessfully accomplish, and had to be repeated. The Figure 3.9 shows the protection that was made to each specimen and the figure 3.10 portrays a broken extremity of the fiber.

Figure 3.9 – Protection made for Optical fibers.

Figure 3.10 - A broken extremity of the Optical fiber.

One of the cases that also occurred, was the fact that sometimes a sample of the optical fiber apparently in good condition, and then when it was done reading the optical signal, it was broken inside, making it impossible proceeding with the test.

Figure 3.11 - Created defect in the test specimens due to the Bostik that was used to protect the fiber.

There was also a defect created in the test specimens due to the Bostik that was used to protect the fiber. This Bostik aimed to protect the optical fiber in the exit of the sample zone so that it does not break after healing. It was tried to minimize this defect, using minimal Bostik possible. In Figure 3.11, it is seen a case in which the specimen was left with a major defect and consequently influence the test results.

Another problem was the adhesion between the thermocouple and the specimen. The adherence is made through the use of adhesive tape to attach the thermocouple to the specimen. Once it wasn't being established a better adhesion between the thermocouple and the specimen, sometimes wasn't checked values of specimen temperature above room temperature. Since the carbon is thermal conductor, it was necessary to place an insulating tape in order to detect hot spots.

There was difficulty in achieving constant and relatively high signal intensity in optical fiber due to the sensitive equipment constituted by systems that could change when they are exposed to noise.

All these difficulties encountered have contributed to the learning of how to proceed when manufacturing this type of samples. Today and after all attempts to manufacture test specimens with optical fibers and defect embedded it is known what must be done to prevent all these problems found during the experimental procedure.

Chapter 4- Results and Analysis

4.1 Experimental results

4.1.1 Static tests

The fatigue tests were performed using a sinusoidal loading for the minimum stress level, 70% of the ultimate strength value that was determinate in the static tests. Figure 4.1 shows the flexural strength in order to the displacement for the specimen without defect or optical fiber. At Figure 4.2, the flexural strength in order to the displacement for the specimens with defect and optical fiber are presented.

The values for the Elastic Modulus (E) and the maximum strength resistance (σ) are obtained from the equations (1) and (2):

$$E = \frac{3 * P * S}{2 * w * t^2 * \varepsilon} \quad (1)$$

$$\sigma = \frac{3 * P * S}{2 * w * t^2} \quad (2)$$

The applied load represented by P, S is the distance between supports, w is the specimen width, t is thickness and ε is the strain obtained from the control software of the test system. After the static tests and the analysis of the results obtained, dynamic testing was done for different values of percentage for minimum flexural strength (60%, 70% and 75%). It was chosen the 70% of the ultimate strength value. For this case, the laminate will have an increase in temperature for a reasonable time test (around 30000 cycles). This way the laminate is subjected to mechanical fatigue and thermal fatigue at the same time

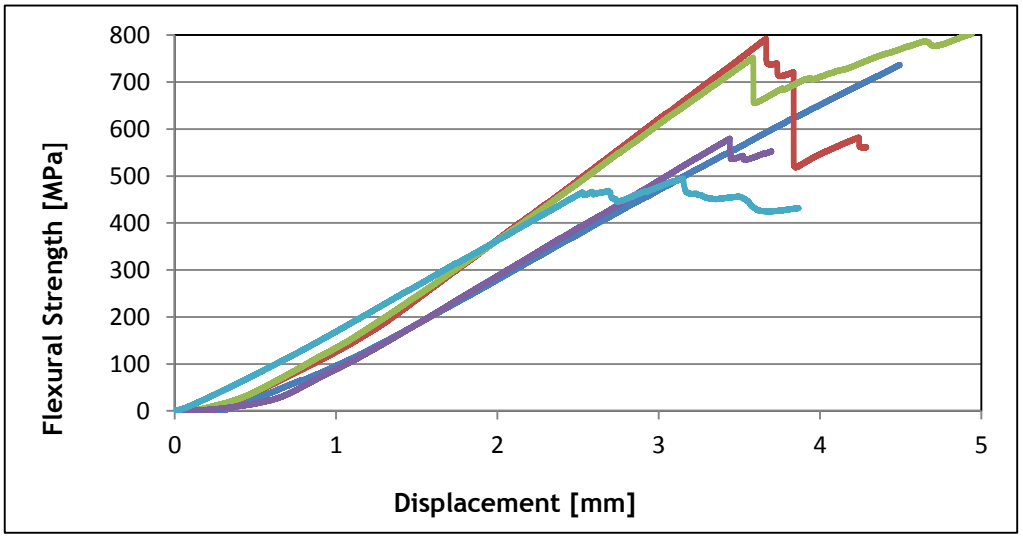

Figure 4.1 - Flexural strength in order to the displacement for the specimen without defect or optical fiber.

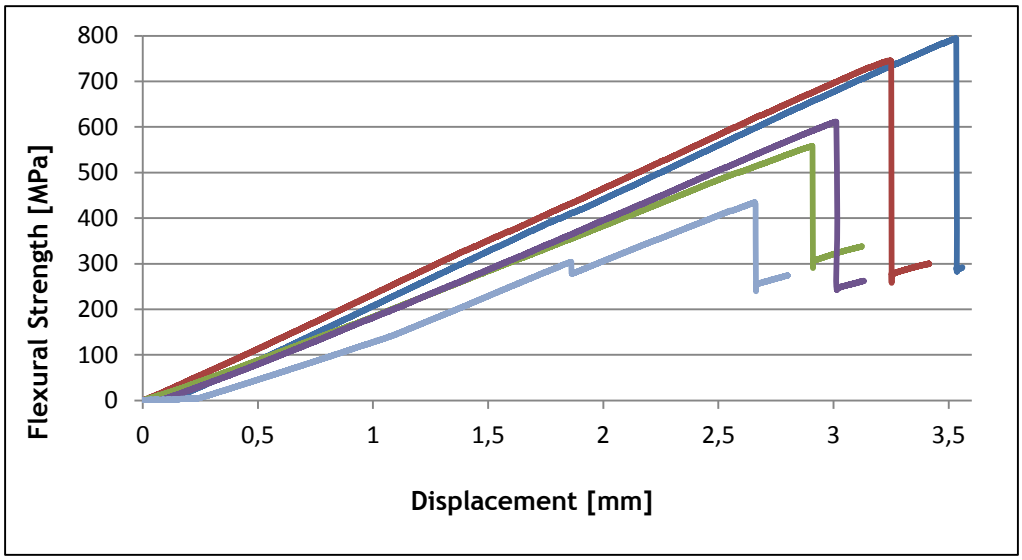

Figure 4.2 - Flexural strength in order to the displacement for the specimen With defect and optical fiber.

Tables 4.1 and 4.2 illustrate the maximum values of flexural strength and respective displacement values to which they occur, in case of the specimens with defect and OF and the simple specimens, in other words without defect and OF.

Table 4.1 - Maximum values for flexural strength and its respective displacement values for the specimens with defect and optical fiber.

Specimen	*Flexural Strength [MPa]*	*Displacement [mm]*
1	791.2	3.51
2	745.1	3.24
3	605.1	2.98
4	575.9	2.83
5	429.7	2.63

Table 4.2 - Maximum values for flexural strength and its respective displacement values for the specimens without defect and optical fiber.

Specimen	*Flexural Strength [MPa]*	*Displacement [mm]*
1	808.0	4.91
2	789.2	3.65
3	744.7	3.55
4	575.2	3.42
5	492.6	3.14

It can be seen that the simple specimen exhibit higher maximum values for flexural strength than those specimens with the defect and OF embedded. When comparing both values of maximum flexural strength, it is concluded that the maximum values, in the case of simple specimens, occur to displacement values higher than those of the specimens without OF and defect.

4.1.2 Fatigue tests

To proceed with the dynamic tests, it was necessary to stipulate the value of the frequency. It has been decided to use a 10 Hz frequency, after submit the sample to different frequencies (6, 10 and 20 Hz). The selection of 10Hz due to the observation of changes in temperature after several thousands of cycles (near 30000). To 6 Hz, trials with more than 500000 cycles showed no significant temperature changes.

At Figure 4.3, it can be seen the elastic modulus variation in order to the number of the cycles and at the Figure 4.4, it can be visualized the variation of the temperature in order to the number of the cycles, for the two different frequencies. Through analysis of these figures, it can be seen that for the frequency of 10Hz, the elastic modulus variation decreases and there is an increase of the variation of temperature.

The value of the frequency of 10 Hz was chosen for being a value that approximates the reality that an aircraft component may be subjected.

It was observed that the frequency influences the fatigue life of the composite, since the test frequency increase, the life of the material decreased, due to greater heat generation by hysteresis. Since the viscoelastic effect and the time available to dissipate heat is reduced, there is a change in the type of fatigue from mechanical fatigue crack initiation and propagation to fatigue caused by the heating effect of the matrix.

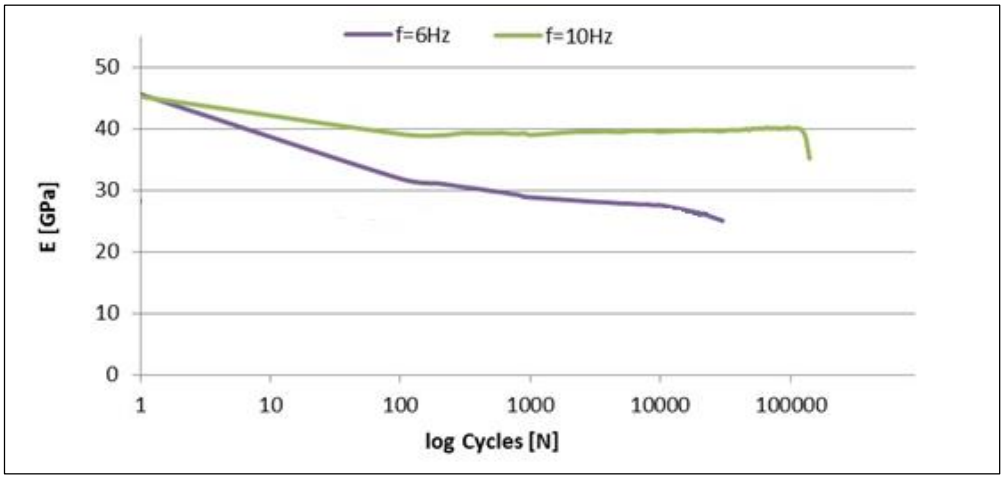

Figure 4.3 – Elastic Modulus variation for two different frequencies.

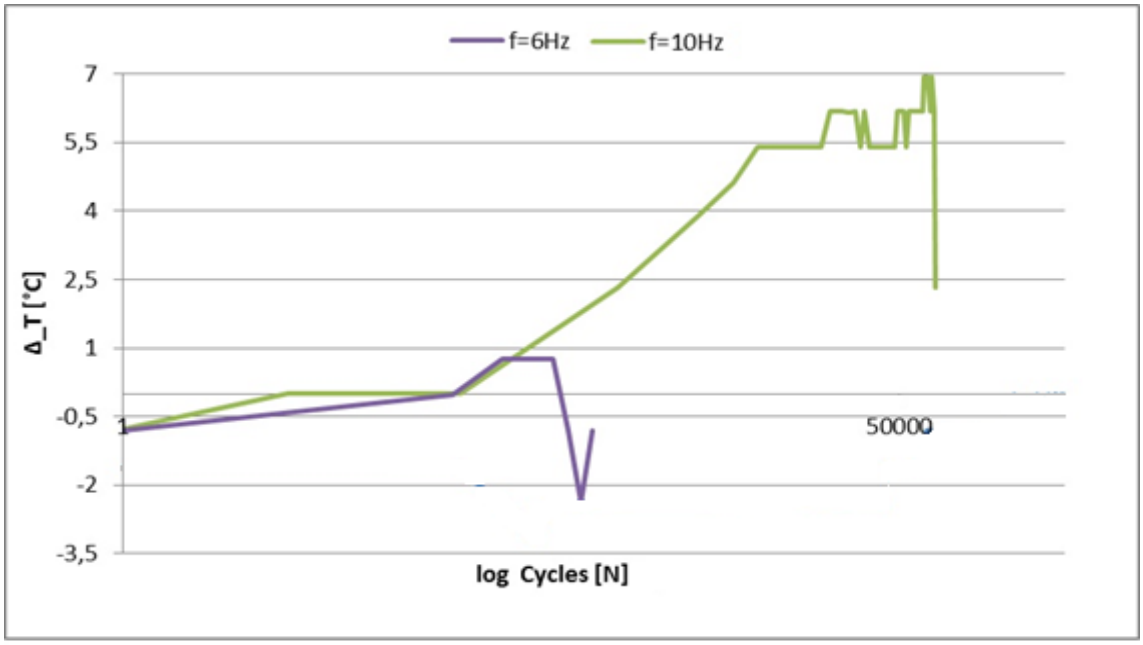

Figure 4.4 – Variation of the temperature for the two different frequencies.

After being subject to the thermal shock cycles between the values of -25° C to 80° C the test pieces were subjected to dynamic testing. In Figures 4.5 and 4.6, it can be observed the elastic modulus variation and the temperature variation in fatigue tests for the specimen subjected to sixty thermal cycles, thirty thermal cycles and without cycles of degradation.

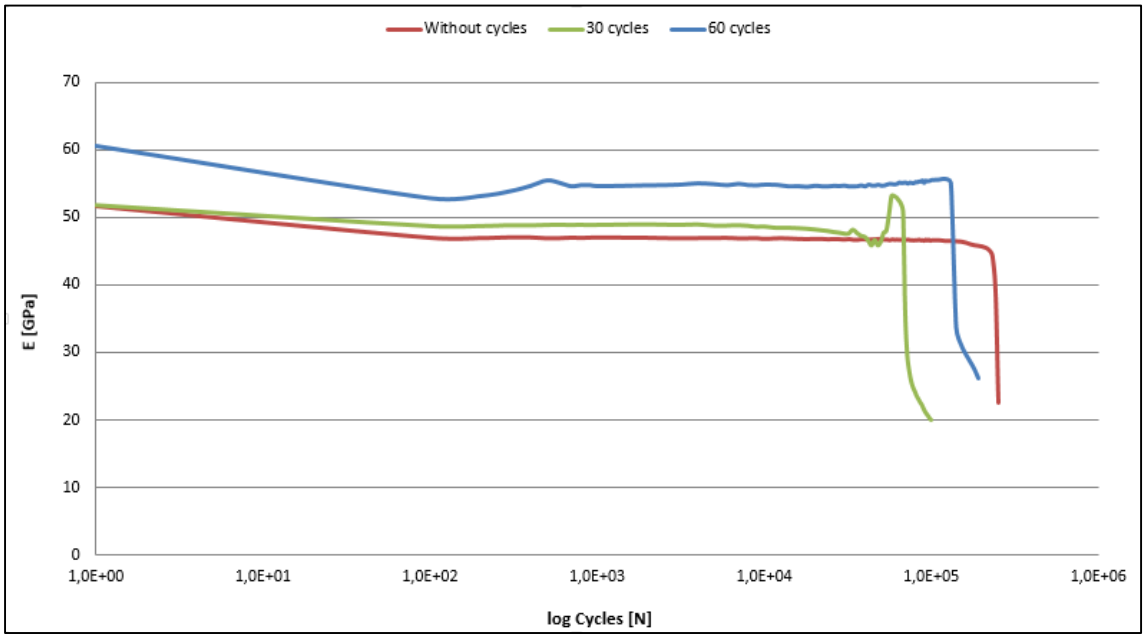

Figure 4.5 - Elastic Modulus variation for three types of degradation of the specimen.

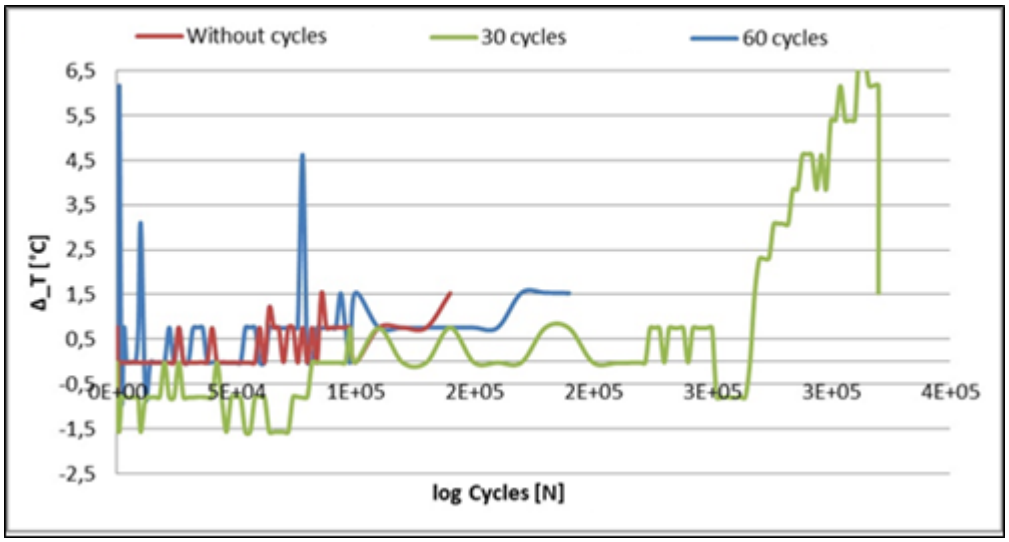

Figure 4.6 - Temperature variation for three types of degradation of the specimen.

Through the analysis of graphs, it was possible to observe that specimen with 30 cycles of temperature presents higher values of temperature changes when compared with the specimens with 60 cycles of temperature and the specimen without temperature cycles. The test results without thermal cycles and 60 cycles may be masked due to poor isolation of the sample.

When looking at Figure 4.6 it can be seen that the specimen without cycles of temperature presents the lowest elastic modulus value. The sample with 30 cycles of temperature proved to be more resistant than others, since it endured more cycles than others.

In the table 4.3, it is showed that the sample without cycles of ageing has significant decrease of the variation of the temperature. Also the difference between the two samples with 30 and 60 cycles of ageing in terms of the variation of the temperature is small, and the sample with more cycles of ageing show higher temperature variation. The young modules shows the same tendency, a decreasing of the performance of the test sample comparing the sample with and without cycles of ageing.

Table 4.3-Elastic Modulus and Temperature variation for the specimens with 60, 30 and without cycles of ageing.

Type of specimens	*ΔE [%]*	*ΔT [%]*
Without cycles of ageing	-22.25	0.26
30 Cycles of ageing	-69.55	22.33
60 Cycles of ageing	-56.86	25.12

The value of elastic modulus variation for the case of 30 cycles of ageing is higher than 60 cycles of ageing. The opposite would be expected, since the more degraded is the sample, the greater the decrease in the variation of the elastic modulus. For this case the tendency has not occurred since the specimen with 60 cycles of ageing endured 190000 cycles, while the sample

with 30 cycles of ageing endured 320000 cycles. If the test piece subjected to 60 cycles of ageing had more time subject to test and had not come into rupture would present a higher elastic modulus value and the tendency occurs.

It was also expected that the elastic modulus variation value for the specimen which was not degraded was the smallest. For this case the rupture occurred at the end of 140,000 cycles of time.

It is concluded from the analysis of table 4.3 that the greater the degradation of the specimen, the greater the variation between room temperature and temperature of the specimen when it is subjected to cyclic loading. The value of temperature variation for the case of the specimen without degradation is very small. Although expected to be a lower value than the degraded samples, there was noted almost no change in temperature. The value of the specimen temperature is usually lower than the room temperature. This was especially because of adhesion of the thermostat to the specimen that proved not to be the best, since the bond between them is taking off, when the specimen was subjected to cyclic loadings. Once the carbon is thermal conductor, the heat dissipates quickly. This forced the outer face of the isolation to detect hot spots outside. For this reason it was not taken the correct reading of the temperature and the value presented in Table 4.3 is not very realistic.

The elastic modulus variation and the temperature variation between four tests specimens are shown in Figures 4.7 and 4.8, respectively.

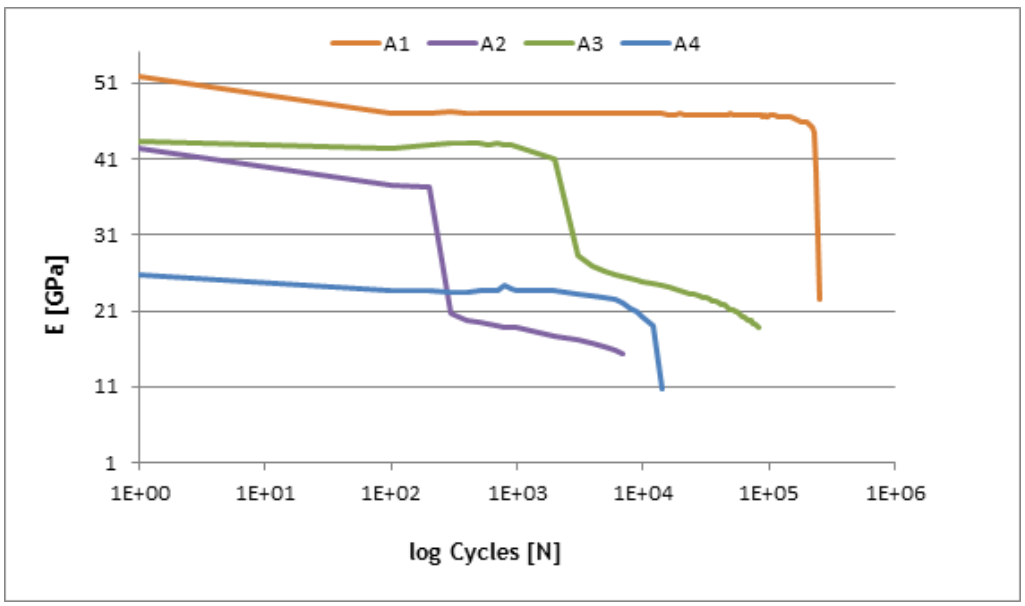

Figure 4.7 - Elastic Modulus variation in fatigue tests.

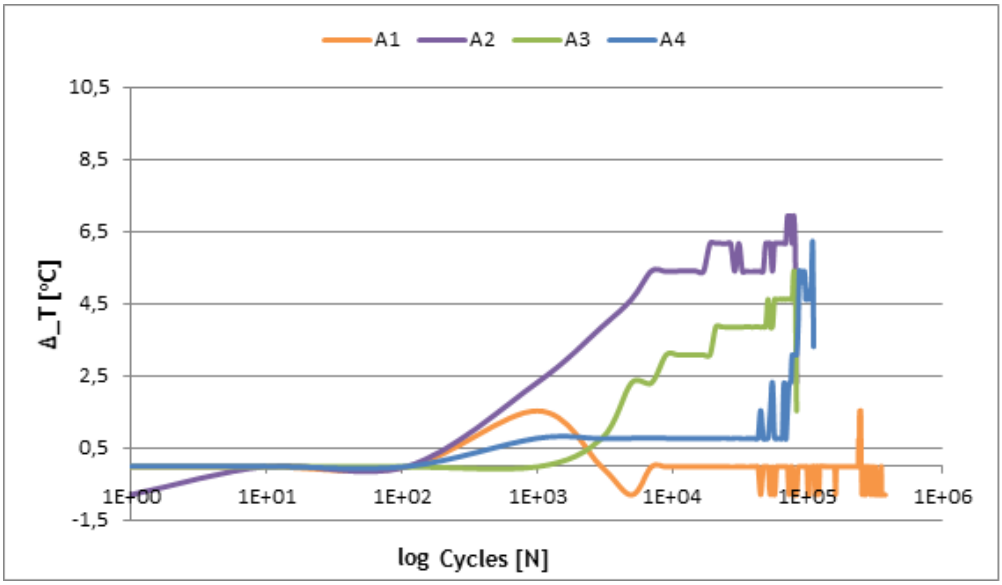

Figure 4.8 – The variation of the temperature in fatigue tests.

The elastic modulus variation and the temperature variation between four tests specimens is important to keep at minimum, this ensures a reliable procedure in the analysis of the results, and is the purpose of table 4.4. The variance between the four specimens isn't significant, as showed in the table.

Table 4.4- Elastic Modulus and Temperature variation for the 4 specimens.

Type of specimens	*ΔE [%]*	*ΔT [%]*
A1	-56.41	-50.65
A2	-42.73	44.67
A3	-56.71	28.70
A4	-63.83	53.81

There is a decrease in stiffness for each specimen. Table 4.4 shows that from the beginning of the test, until it ends are verified a decrease between 42 and 65% of the stiffness of the specimens.

In the case of temperature variation, there is an increase in this value for 3 of the 4 cases tested. Was noted an increase for 3 samples between 28 and 54% of the temperature variation. For one of the specimens, there was a decline in the value of temperature. This may be due to the adhesion between the thermostat and the specimen. Once it was not be established a better adhesion between the thermostat and the specimen rarely checked values of specimen temperature above room temperature.

Figure 4.9 shows the total countdowns from the AE tests.

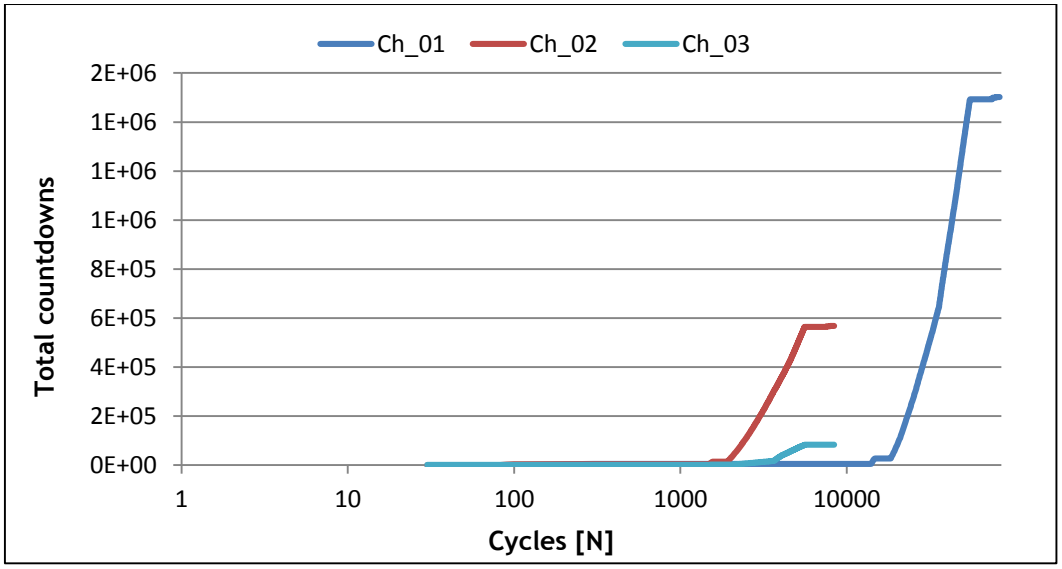

Figure 4.9 - Acoustic emission intensity.

The results obtained allow identifying the damage evolution, following a nonlinear tendency starting from low levels occurrences, as matrix cracking, and ending with high intensity catastrophic events, such delamination or a large number of fiber breakages, prior to give the final material rupture.

This figure shows that when the temperature rises (see Figure 4.8) increases the noise within the laminate in this way it is proved that the increase in temperature is related to the growth of the damage.

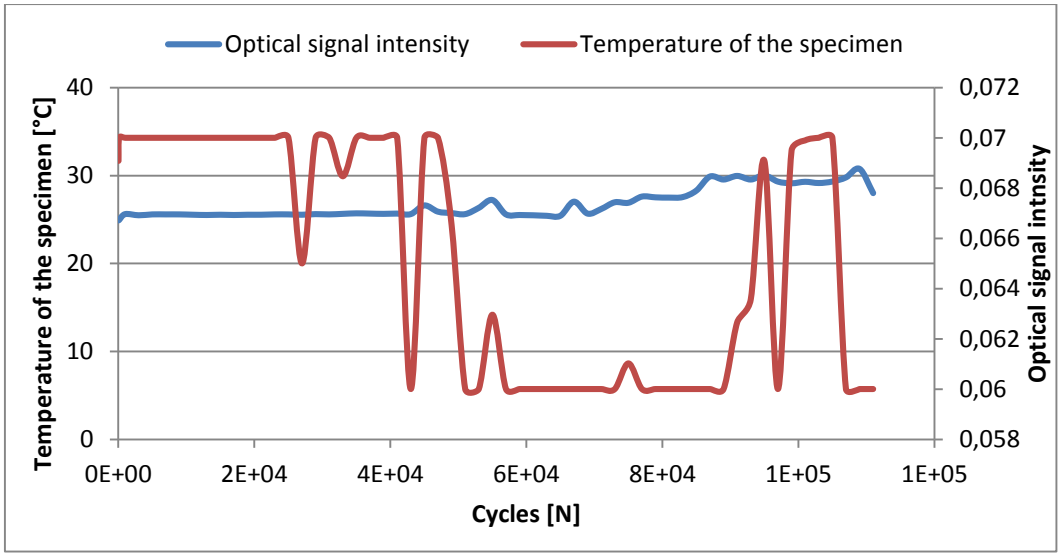

Figure 4.10 - Optical signal intensity Vs Temperature of the specimen.

In the Figure 4.10 are represented the temperature of the specimen and the intensity of the optical signal in order to the number of cycles. Through the visualization of this figure, can be see that there are throughout the test, a large variation of the specimen temperature.

Although it can be seen that there is some intensity of the optical signal, especially when there is large variations in the specimen temperature, these values are not as expected. Would be expected to obtain higher values for the optical signal intensity. These results show that during the test, the difficulties faced, adversely affected the intensity of the optical signal.

It can be said that this optical fiber is capable of functioning as sensors, when it is subjected to fatigue, despite not being the best in this case. By making changes in order to avoid all the difficulties encountered throughout the manufacturing process, can get a better signal and consequently will have a better sensor, when the specimen is subjected to fatigue.

Chapter 5- Conclusions and future works

5.1 Final conclusions

In order to study the feasibility of monitoring structures, by inserting simple optical fibers as sensors, when they are subject to fatigue, it was construed and tested the specimens and it was been conclude that a simple optical fiber can be used as a sensor, when subjected under cycling loading.

By the results obtained, it was observed a decrease in the modulus of elasticity in order to the number of cycles. Meanwhile, there is an increase of temperature. Through visualization of the results of acoustic emission, it could be seen that there are changes to whenever there is a variation in temperature thus making it possible to use an optical sensor (with many advantages) for detecting a critical damage. Once the carbon has a good thermal conductivity it isn't viewed high temperature variations along the test. The geometry of the specimen also contributes to a high dissipation of thermal energy.

The value of the specimen temperature is usually lower than the room temperature. This was especially because of adhesion of the thermostat to the specimen that proved not to be the best, since the bond between them is taking off, when the specimen was subjected to cyclic loadings and due to the fact that room temperature is to be measured near the oil tank and with time it warms up. For these reasons it was not taken the correct reading of the temperature.

From the total countdowns from the AE tests. The results obtained allow identifying the damage evolution, following a nonlinear tendency starting from low levels occurrences, as matrix cracking, and ending with high intensity catastrophic events, such delamination or a large number of fiber breakages, prior to give the final material rupture.

Even the results are not the best, for example it can be seen that there is some intensity of the optical signal during the fatigue tests, especially when there is large variations in the specimen temperature, these values are not as expected. It can be said that this optical fiber is capable of functioning as sensors, when it is subjected to fatigue, despite not being the best in this case. By making changes in order to avoid all the difficulties encountered throughout the manufacturing process, it can get a better signal and consequently will have a better sensor, when the specimen is subjected to fatigue.

It was observed that the frequency influences the fatigue life of the composite, since the test frequency increase, the life of the material decreased, due to greater heat generation by hysteresis. Since the viscoelastic effect and the time available to dissipate heat is reduced,

there is a change in the type of fatigue from mechanical fatigue crack initiation and propagation to fatigue caused by the heating effect of the matrix.

The results are a consequence of the many difficulties that occur. The process of manufacture, the data acquisition, and the system of temperature reading, the tests performed are an important part of the process of get results and demonstrated not be easy to achieve during the whole experimental work. Throughout the experimental work it was observed a high sensitivity at the test conditions, from room temperature during the test, the geometry of the specimens, the placement of the thermocouple, the isolation of the outer face of the laminate, etc.

Once it occurred many problems during this experimental work, it can be said that with the right modifications it can be achieved better results and consequently a monitorization system more reliable.

5.2 Recommendations for future works

For the future, the same procedure for another type of fiber could be realized.

The geometry of the specimen could be changed. Since the smaller area of the specimen, and since the carbon fiber is being used, the faster heat dissipation occurs and will eventually not a change in temperature. The minimum width should be close to 40 mm so that the heat dissipation is not too fast.

Simulation and structural analysis programs can also be used to study different types of configurations for the sample in order a characterization of the specimen was taken before being experimentally performed.

Experimental tests should guarantee that the test temperature is constant.

The analysis of the optical signal must be made with a spectrometer to assess any changes in wavelength of the signal.

The light source should not be just red light (He-Ne laser with wavelength 632,8 nm. Temperature can be affected by different ranges of colors of light and the red color can even be weakly influenced by temperature.

References

[1] "Composite Materials." [Online]. Available: http:// en.wikipedia.org/wiki /Composite_material#mediaviewer/File:Composite_3d.png. [Accessed: 31-May-2014].

[2] P. A. G. Vieira, "Current Airframe Manufacturing Technologies in the Aeronautical Industry and Trends for Future Developments," 2013.

[3] "Materiais compósitos na aviação." [Online]. Available: http:// www.engenhariae.com.br/ tecnologia/ materiais-compositos-na-aviacao/. [Accessed: 31-May-2014].

[4] "Carbon fiber plastic composite tailfin for a radio-controlled helicopter model." [Online]. Available: http:// en.wikipedia.org/ wiki/ Composite_material# mediaviewer/ File:Cfk_heli_slw.jpg. [Accessed: 31-May-2014].

[5] "Enhanced Adaptive Droop Nose technology integration." [Online]. Available: http://en.wikipedia.org/wiki/Smart_Intelligent_Aircraft_Structures#mediaviewer/File :Enhanced_Adaptive_Droop_Nose_technology_integration.jpg. [Accessed: 20-Aug-2014].

[6] S. Minakuchi and N. Takeda, "Recent advancement in optical fiber sensing for aerospace composite structures," *Photonic Sensors*, vol. 3, no. 4, pp. 345–354, Oct. 2013.

[7] "Structural Health Monitoring for Commercial Space Vehicles." [Online]. Available: http://www.parabolicarc.com/2013/09/24/flight-opportunities-program-flight-set-october/. [Accessed: 31-May-2014].

[8] C. Y. Huang, R. S. Trask, and I. P. Bond, "Characterization and analysis of carbon fibre-reinforced polymer composite laminates with embedded circular vasculature.," *J. R. Soc. Interface*, vol. 7, no. 49, pp. 1229–41, Aug. 2010.

[9] J. M. López-higuera, S. Member, L. R. Cobo, A. Q. Incera, and A. Cobo, "Fiber Optic Sensors in Structural Health Monitoring," vol. 29, no. 4, pp. 587–608, 2011.

[10] "No Title." [Online]. Available: http://www.owi-lab.be/content/state-art-and-new-developments-field-structural-health-monitoring.

[11] D. Sheet, A. P. Texipreg, and A. Sporting, "Rem m p," no. Mi, pp. 12–15, 2002.

[12] B. Marques, A. P. Silva, P. N. B. Reis, T. C. Devezas, and L. Freitas, "Monitorização de Dano em Laminados Compósitos através de Sensores Óticos," 2013.

[13] H. Tsutsui, A. Kawamata, T. Sanda, and N. Takeda, “Detection of impact damage of stiffened composite panels using embedded small-diameter optical fibers,” *Smart Mater. Struct.*, vol. 13, no. 6, pp. 1284–1290, Dec. 2004.

[14] B. Michael, “Smart structures through embedding optical fibre strain sensing,” no. May, 2001.

[15] S. Takeda, Y. Okabe, and N. Takeda, “Delamination detection in CFRP laminates with embedded small-diameter fiber Bragg grating sensors,” *Compos. Part A Appl. Sci. Manuf.*, vol. 33, no. 7, pp. 971–980, Jul. 2002.

[16] B. Benchekchou and R. G. White, “Stresses around fasteners in composite structures in flexure and effects on fatigue damage initiation part 2: countersunk bolts,” *Compos. Struct.*, vol. 33, no. 2, pp. 109–119, Jan. 1995.

[17] K. Diamanti and C. Soutis, “Structural health monitoring techniques for aircraft composite structures,” *Prog. Aerosp. Sci.*, vol. 46, no. 8, pp. 342–352, Nov. 2010.

[18] W. F. Smith, *Princípios de Ciência e Engenharia dos Materiais*, 3rd ed. McGraw-Hill, 1996, pp. 767–781.

[19] A. M. P. da Silva, “UNIVERSIDADE DA BEIRA INTERIOR Departamento de Engenharia Electromecânica Estudo do Comportamento de Material Compósito Inteligente em Impacto de Baixa Velocidade,” 1999.

[20] “Thermoplastics composites in construction.” [Online]. Available: http:// theconstructor.org/composite/thermoplastic-composites-in-construction/1479/. [Accessed: 28-May-2014].

[21] A. Chambers, M. Mowlem, and L. Dokos, “Evaluating impact damage in CFRP using fibre optic sensors,” *Compos. Sci. Technol.*, vol. 67, no. 6, pp. 1235–1242, May 2007.

[22] B. Riccio, A.; Caprio, F. di; Camerlingo, F; Scaramuzzino, F. and Gambino, “Positioning of embedded optical fibres sensors for the monitoring of buckling in stiffened composite panels,” *Appl. Compos. Mater.*, 2012.

[23] R. Starikov and J. Scho, “Local fatigue behaviour of CFRP bolted joints,” vol. 62, pp. 243–253, 2002.

[24] J. Ferreira, P. Reis, J. Costa, and M. Richardson, “Fatigue behaviour of Kevlar composites with nanoclay-filled epoxy resin,” *J. Compos. Mater.*, vol. 47, no. 15, pp. 1885–1895, Jun. 2012.

[25] J. R. Tarpani, M. Angeloni, L. Iezzi, and C. E. G. De Castro, “Fadiga Após Múltiplos Impactos Em Laminados Carbono-Epóxi,” *Tecnol. em Metal. e Mater.*, vol. 2, no. 4, pp. 63–70, 2006.

[26] S. Takeda, S. Minakuchi, Y. Okabe, and N. Takeda, “Delamination monitoring of laminated composites subjected to low-velocity impact using small-diameter FBG sensors,” *Compos. Part A Appl. Sci. Manuf.*, vol. 36, no. 7, pp. 903–908, Jul. 2005.

[27] H. J. D. Correia and T. C. Devezas, “Comportamento mecânico em flexão dos compósitos carbono/resina epoxídica com fibras ópticas incorporadas,” 2000, pp. 230–237.

[28] J. M. a. Silva, J. a. M. Ferreira, and T. C. Devezas, “Fatigue damage of carbon–epoxy laminates with embedded optical fibres,” *Mater. Sci. Technol.*, vol. 19, no. 6, pp. 809–814, Jun. 2003.

[29] A. P. Silva and T. C. Devezas, “Resistência ao impacto de compósitos com a inserção de fibras ópticas,” 2000, pp. 238–247.

[30] A. K. Noor, S. L. Venneri, D. B. Paul, and M. a. Hopkins, “Structures technology for future aerospace systems,” *Comput. Struct.*, vol. 74, no. 5, pp. 507–519, Feb. 2000.

[31] J.-M. Henault, G. Moreau, S. Blairon, J. Salin, J.-R. Courivaud, F. Taillade, E. Merliot, J.-P. Dubois, J. Bertrand, S. Buschaert, S. Mayer, and S. Delepine-Lesoille, “Truly Distributed Optical Fiber Sensors for Structural Health Monitoring: From the Telecommunication Optical Fiber Drawling Tower to Water Leakage Detection in Dikes and Concrete Structure Strain Monitoring,” *Adv. Civ. Eng.*, vol. 2010, pp. 1–13, 2010.

[32] B. Fernando, G. F. and Degamber, “Process of monitoring of fibre reinforced composites using optical fibre sensors,” *Int. Mater. Rev.*, vol. 51, no. 2, pp. 65–105, 2006.

[33] R. O. Claus, K. D. Bennett, a. M. Vengsarkar, and K. a. Murphy, “Embedded optical fiber sensors for materials evaluation,” *J. Nondestruct. Eval.*, vol. 8, no. 2, pp. 135–145, Jun. 1989.

[34] K. Hotate, “Fiber optic distributed sensing for smart structures and smart materials,” *Dig. 9th Int. Conf. Opt. Internet (COIN 2010)*, pp. 1–3, Jul. 2010.

[35] D. C. Seo and J. J. Lee, “Effect of embedded optical fiber sensors on transverse crack spacing of smart composite structures,” *Compos. Struct.*, vol. 32, no. 1–4, pp. 51–58, Jan. 1995.

[36] P. Antunes, H. Lima, H. Varum, and P. André, “Optical fiber sensors for static and dynamic health monitoring of civil engineering infrastructures: Abode wall case study,” *Measurement*, vol. 45, no. 7, pp. 1695–1705, Aug. 2012.

[37] A. Cusano, P. Capoluongo, S. Campopiano, A. Cutolo, M. Giordano, M. Caponero, F. Felli, and A. Paolozzi, “Dynamic measurements on a star tracker prototype of AMS using fiber optic sensors,” *Smart Mater. Struct.*, vol. 15, no. 2, pp. 441–450, Apr. 2006.

[38] G. F. Fernando, “Fibre optic sensor systems for monitoring composite structures,” 2005, no. December, pp. 41–49.

[39] D. C. Lee, J. J. Lee, and S. J. Yun, “The mechanical characteristics of smart composite structures with embedded optical fiber sensors,” vol. 32, pp. 39–50, 1995.

[40] R. Jones and S. Galea, “Health monitoring of composite repairs and joints using optical fibres,” *Compos. Struct.*, vol. 58, no. 3, pp. 397–403, Nov. 2002.

[41] N. Olson, C. K. Y. Leung, and A. Meng, “Crack sensing with a multimode fiber: experimental and theoretical studies,” *Sensors Actuators A Phys.*, vol. 118, no. 2, pp. 268–277, Feb. 2005.

[42] N. Takeda, “Summary report of the structural health-monitoring project for smart composite structure systems,” *Adv. Compos. Mater.*, vol. 10, no. 2–3, pp. 107–118, Jan. 2001.

[43] N. Takeda, “Characterization of microscopic damage in composite laminates and real-time monitoring by embedded optical fiber sensors,” *Int. J. Fatigue*, vol. 24, no. 2–4, pp. 281–289, Apr. 2002.

[44] H. Murayama, D. Wada, and H. Igawa, “Structural health monitoring by using fiber-optic distributed strain sensors with high spatial resolution,” *Photonic Sensors*, vol. 3, no. 4, pp. 355–376, Oct. 2013.

[45] J. S. Leng and A. Asundi, “NDE of smart structures using multimode ® ber optic vibration sensor,” vol. 35, pp. 45–51, 2002.

[46] B. Benchekchou and N. S. Ferguson, “The effect of embedded optical fibres on the fatigue behaviour of composite plates,” *Compos. Struct.*, vol. 41, no. 2, pp. 113–120, Feb. 1998.

[47] T. H. Loutas, a. Panopoulou, D. Roulias, and V. Kostopoulos, “Intelligent health monitoring of aerospace composite structures based on dynamic strain measurements,” *Expert Syst. Appl.*, vol. 39, no. 9, pp. 8412–8422, Jul. 2012.

[48] J. A. M. Silva, José M. A.; Devezas, Tessaleno C.; Silva, Abílio P. and Ferreira, “Mechanical characterization of composites with embedded optical fibers,” *J. Compos. Mater.*, vol. 39, pp. 1261–1281, 2005.

[49] T. C. Silva, J.M.A.;Ferreira, J. M. A.; Silva, Abílio P. and Devezas, “Mechanical characterization of composites with embedded optical fibers,” *Compos. Mater.*, vol. 39, pp. 1261–1281, 2005.

[50] A. Panopoulou, T. Loutas, D. Roulias, S. Fransen, and V. Kostopoulos, “Dynamic fiber Bragg gratings based health monitoring system of composite aerospace structures,” *Acta Astronaut.*, vol. 69, no. 7–8, pp. 445–457, Sep. 2011.

[51] X. and Z. L. Yuan, Shenfang; Lai, Xiaosong; Zhao, Xia; Xu, “Distributed structural health monitoring system based on smart wireless sensor and multi- agent techonology,” *Smart Mater. Struct.*, no. 15, pp. 1–8, 2006.

[52] L. M. Zhou, G. and Sim, “Damage detection and assessment in fibre-reinforced composite structures with embedded fibre optic sensors-review,” *Smart Mater. Struct.*, no. 11, pp. 925–939, 2002.

[53] A. Panopoulou, S. Fransen, V. Gomez-Molinero, and V. Kostopoulos, “Experimental modal analysis and dynamic strain fiber Bragg gratings for structural health monitoring of composite antenna sub-reflector,” *CEAS Sp. J.*, vol. 5, no. 1–2, pp. 57–73, Jul. 2013.

[54] P. Capoluongo, C. Ambrosino, S. Campopiano, a. Cutolo, M. Giordano, I. Bovio, L. Lecce, and a. Cusano, “Modal analysis and damage detection by Fiber Bragg grating sensors,” *Sensors Actuators A Phys.*, vol. 133, no. 2, pp. 415–424, Feb. 2007.

[55] J. H. Mao, W. L. Jin, Y. He, D. J. Cleland, and Y. Bai, “A novel method of embedding distributed optical fiber sensors for structural health monitoring,” *Smart Mater. Struct.*, vol. 20, no. 12, p. 125018, Dec. 2011.

[56] I. Kressel, “Fiber optic based techonology for UAV structural health monitoring,” in *27th ICAF Symposium*, 2013.

[57] “Analogy between the operation of the human nervous system and of a structure SHM.” [Online]. Available: http://www.owi-lab.be/content/state-art-and-new-developments-field-structural-health-monitoring. [Accessed: 02-Jun-2014].

Annex A - Datasheet Prepreg TEXIPREG® REM

SEAL

20025 Legnano (MI) - ITALY
Tel. +39-0331-467.555 fax.: +39-0331-467.777
e mail: info.IT@seal.it web site: www.seal.it

Data Sheet of Advanced Prepreg TEXIPREG® REM

REM MATRIX PREPREGS

DESCRIPTION

REM a transparent epoxy matrix, suitable to impregnate carbon, glass fabric and unidirectional. It could be processed both for hot press and vacuum bag cure. It has satisfactory self adhesive properties and is particulary suited for manufacturing visible parts.

APPLICATIONS

Automotive Sporting goods Industrial

RESIN PROPERTIES

Typical Prepreg Properties:	*Unit*	*Typical values*
Outlife @ 23°C	days	30
Storage life @ -18°C	months	12
Cured resin density	g/cc	1.2
Tg fully cured	°C	130
Gel time @125°C	min	12'00"±3'00"

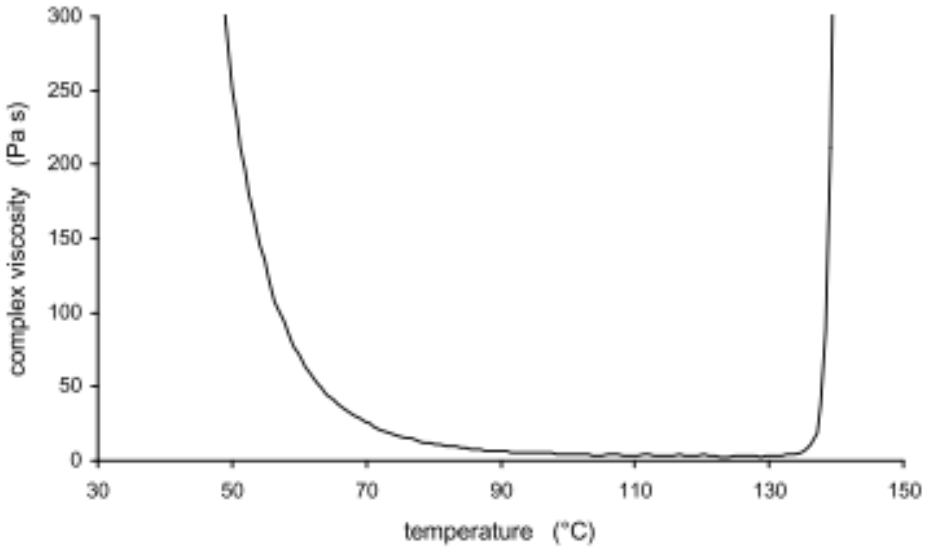

In the figure is shown the rheological profile of REM resin (freq. 1Hz, plate-plate, heat up rate 3°C/min)

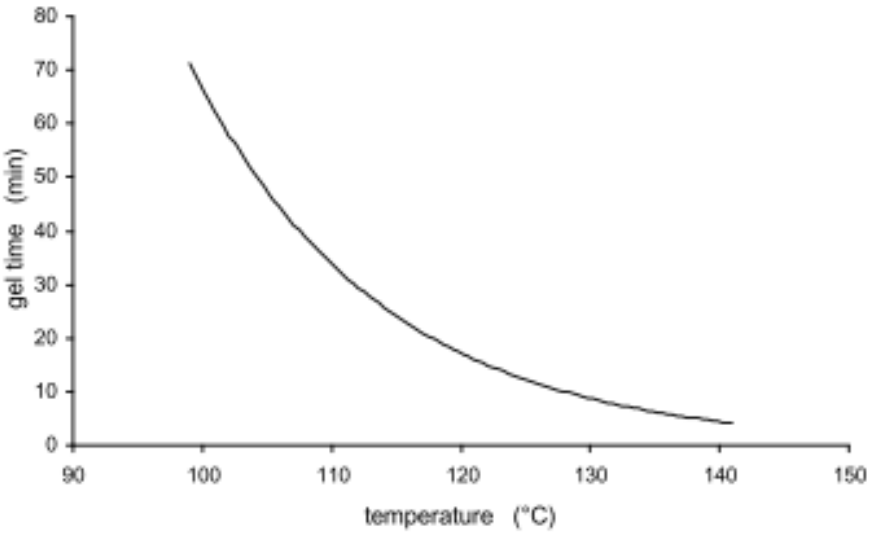

In the figure is shown the Gel Time profile of REM resin

SEAL
20025 Legnano (MI) - ITALY
Tel. +39-0331-467.555 fax.: +39-0331-467.777
e mail: info.IT@seal.it web site: www.seal.it

PROCESSING

Prepreg made from REM resin can be processed by hot plate press, in autoclave and in oven (vacuum bag molding). It should be cured at 125°C for 60 minutes

Curing Temperature	Curing Time
125°C	60 minutes

compression moulding:

- put the packet into the mould at room temperature
- close the mould and apply a pressure about 1 bar
- heat to 125 °C at a 3-5 °C/min rate
- when 120-125 °C is reached apply 2-7 bar
- maintain pressure and Temperature for 60'
- get the part out from the mould

autoclave/vacuum-bag moulding:

- make the bag and apply 0.5 bar vacuum
- heat to 125 °C at a 3-5 °C/min rate
- when 120-125 °C is reached apply 2-7 bar
- maintain pressure and Temperature for 60'
- cool to room temperature under pressure
- get the part out from the mould

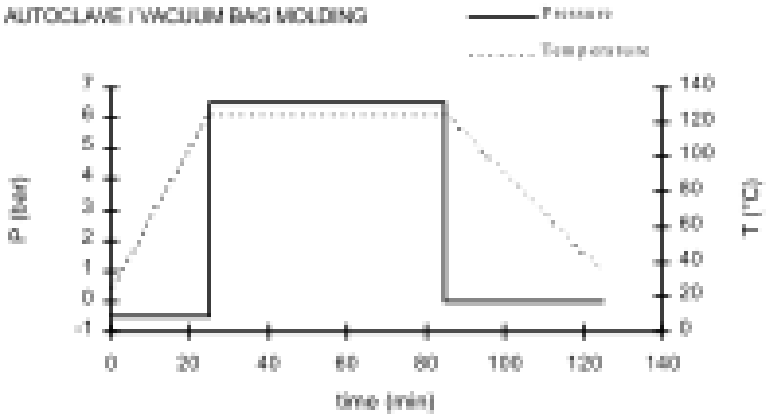

SEAL
29025 Legnano (MI) - ITALY
Tel. +39-0331-467.555 fax: +39-0331-467.777
e mail: info.IT@seal.it web site: www.seal.it

DELIVERY FORM & PACKAGING

The prepreg fabrics are rolled on 75 mm of diameter cardboard cores with release paper on one side and polyethylene film separator on the other side.
It is delivered on rolls sealed in waterproof plastic bag and packed in cardboard boxes.

Standard width: 100 cm
Standard length: 50 m

The prepreg UD are rolled on 300 mm of diameter cardboard cores with release paper on one side (or no flat polyethylene film as alternative) and no flat polyethylene film separator on the other side.
It is delivered on rolls sealed in waterproof plastic bag and packed in cardboard boxes.

Standard width: 60 cm
Standard length: 100 m

HANDLING & STORAGE

Stock rolls at -18 °C, sealed in original packages.
Shop life at 23°C refers to rolls sealed in original packages.
Before the use of the prepreg, get out the roll from the freezer and let it warm up to room temperature for 6 hours sealed in its original package.

SAFETY HAZARD

This product contains epoxy resin.
May cause allergic reaction.
Avoid prolonged contact with skin.
The use of latex gloves for handling is suggested.
It is also suggested to work in an aerated environment.
Scraps are to be cured and discarded following national law.

Note
For further information check the Material Safety Data Sheet

Annex B - Properties of the optical fiber used

Multimode Fiber

Model	Operating Wavelength (nm)	NA	Core Diameter (µm)	Cladding Diameter (µm)	Coating Diameter (µm)	Remark
F-MSD	850/1300	0.200	50 ±3	125 ±2	250 ±15	Graded index, communication
F-MSD-C	850/1300	0.200	50 ±3	125 ±2	250 ±15	Graded index, communication
F-MFD	850/1300	0.275	62.5 ±3	125 ±2	250 ±15	Graded index, communication
F-MLD	850/1300	0.290	100 ±4	140 ±3	250 ±15	Graded index
F-MLD-C	850/1300	0.29	100 ±4	140 ±3	250 ±15	Graded index
F-MSD-T	850/1300	0.2	50 ±3	125 ±2	155 ±5	Graded index
F-MFD-T	850/1300	0.275	62.5 ±3	125 ±2	155 ±5	Graded index
F-MLD-T	850/1300	0.29	100 ±4	140 ±3	170 ±5	Graded index
F-MLD-H	850/1300	0.29	100 ±3	140 ±2	172 ±2	Graded index
F-MTC	500-2100	0.22	365 ±10	400 ±10	430 ±30	Step index, high power delivery
F-MFC	500-2100	0.22	550 ±12	600 ±10	630 ±10	Step index, high power delivery
F-MSC	500-1100	0.37	600 ±10	630 ±10	1040 ±30	Step index, medium power delivery
F-MBB	500-1100	0.37	200 ±4	230 +0/-10	500 ±30	Step index
F-MBB-C	500-1100	0.37	200 ±4	230 +0/-10	500 ±30	Step index
F-MBC	500-1100	0.37	400 ±8	430 +5/-10	730 ±30	Step index
F-MSC	500-1100	0.37	600 ±10	630 ±10	1040 ±30	Step index
F-MBE	500-1100	0.37	1000 ±15	1035 ±15	1400 ±50	Step index
F-MCB-T	250-1100	0.22	100 ±3	110 ±3	140 ±5	Step index
F-MCC-T	250-1100	0.22	200 ±5	220 ±5	250 ±5	Step index

Specialty Optical Fiber

Model	Operating Wavelength	Cut-off Wavelength	NA	Cladding Diameter (µm)	Coating Diameter (µm)	Remark
F-SBG-13/15	1310/1550	1100-1260	0.12-0.14	125 ±1	245 ±12	Photosensitive, fiber gratings
F-EDF	980/1550	900-970	0.22-0.24	125 ±1	245 ±12	Rare earth doped, erbium
F-EDF-2	980/1550	870-970	0.21-0.24	125 ±1	245 ±12	Rare earth doped, erbium
F-EDF-5	980/1550	870-970	0.21-0.23	125 ±1	245 ±12	Rare earth doped, erbium
F-EDF-T3		1100-1250	0.21-0.25	125 ±1	245 ±10	Rare earth doped, erbium
F-EDF-T6		1100-1400	0.23-0.27	125 ±1	245 ±10	Rare earth doped, erbium
F-YDC-1100-C	1060-1100	<960	0.06-0.08	270 ±25	400 ±30	Rare earth doped, Ytterbium, dual clas
F-YDC-1100-8/230	1060-1110	<1100	0.1	235 ±5	350 ±15	Rare earth doped, Ytterbium, dual clas
F-CP1100	1075-1100	900	0.12-0.16	125 ±1	245 ±12	Rare earth doped, Ytterbium, dual clas
F-SMM900	1075-1550	850-970	0.24-0.28	125 ±1	245 ±10	Pump delivery
F-DF1500Y	950-1050	950-1050	0.20-0.24	125 ±1	245 ±12	Rare earth doped, Erbium-Ytterbium
F-CP1500Y		1400		125 ±1	245 ±10	Rare earth doped, Erbium-Ytterbium
F-DF1000	875-1025	875-1025	0.18-0.22	125 ±1	245 ±12	Rare earth doped, neodymium

Annex C - MatLab routine

```
%%%%%%%%%%%%%%%%%%%%%%%%%%%%%%%%%%%%%%%%%%%%%%%%
%                                                %
% Aquisição de dados ao longo do tempo           %
%                                                %
%%%%%%%%%%%%%%%%%%%%%%%%%%%%%%%%%%%%%%%%%%%%%%%%
clc
clear

shots = [1 10 89 200*ones(1,250)];
n = 4;                    % ciclos amostrados
f = 6;                    % frequencia de excitação
ts = (1/6)*4/98;          % periodo de amostragem
fs = 1/ts;                % frequencia de amostragem
Nsample = 98;             % numero de amostras recolhidas

% time vector
time_vector = [0:Nsample-1]*n/f/Nsample;

% 1 - Request from user the name of the COM in string format
str = input('Name of the COM - ','s');

% 2 - Serial object creation
s = serial(str);

% 3 - Serial port configuration
set(s,'BaudRate',9600);

% 4 - Save data
file_name = input('File name - ','s');
file_name = [file_name '.xls'];
fileID = fopen(file_name,'w');
fprintf(fileID,'Tempo   Temperatura do Proveto  Temperatura Ambiente
Ensaio\r\n');
fclose(fileID);

for i = shots

  pause(i);

  fopen(s);

  disp('****** EM AQUISIÇÃO ******')
  fwrite(s,'d');
  vector = fread(s,200);
  disp('****** AQUISIÇÃO TERMINADA ******')
  fclose(s)

  temperatura_ambiente =
0.03125*double(typecast(uint8([vector(2),vector(1)]),'int16'))/4;
  c = double(typecast(uint8([vector(4),vector(3)]),'int16'));
  temperatura_proveto = Ktemp(1.024*c/32768,temperatura_ambiente);

  aquisicao = [];
```

```
  coluna = 1;
  for j = [5:2:200]
   aquisicao(1,coluna) =
double(typecast(uint8([vector(j+1),vector(j)]),'int16'));
   aquisicao(1,coluna) = aquisicao(1,coluna)*1.024/2^16;
   coluna = coluna + 1;
  end

  subplot(1,2,1)
    plot(aquisicao,'o-');
    title('Representacao dominio do tempo')
    xlabel('Tempo [seg]')
  subplot(1,2,2)
    NFFT = 2^nextpow2(Nsample);
    Y = fft(aquisicao,NFFT)/Nsample;
    F = fs/2*linspace(0,1,NFFT/2+1);
    plot(F,2*abs(Y(1:NFFT/2+1)))
    title('Representação dominio frequencia')
    xlabel('Frequencia [Hz]')

  fileID = fopen(file_name,'a');
  fprintf(fileID,'ENSAIO');
  fprintf(fileID,'\r\n');
  fprintf(fileID,'%6.2f     ',i);
  fprintf(fileID,'%6.2f     ',temperatura_proveto);
  fprintf(fileID,'%6.2f     ',temperatura_ambiente);
  fprintf(fileID,'%6.2f ',aquisicao');
  fprintf(fileID,'\r\n');

  fprintf(fileID,'FFT   ');
  fprintf(fileID,'%6.2f     ',2*abs(Y(1:NFFT/2+1)));
  fprintf(fileID,'\r\n');
  fprintf(fileID,'Frequência    ');
  fprintf(fileID,'%6.2f     ',F);
  fprintf(fileID,'\r\n');
  fprintf(fileID,'\r\n');

  fclose(fileID);
end

close all
```

Annex D – ASTM D790

Designation: D 790 – 03

Standard Test Methods for Flexural Properties of Unreinforced and Reinforced Plastics and Electrical Insulating Materials[1]

This standard is issued under the fixed designation D 790; the number immediately following the designation indicates the year of original adoption or, in the case of revision, the year of last revision. A number in parentheses indicates the year of last reapproval. A superscript epsilon (ε) indicates an editorial change since the last revision or reapproval.

This standard has been approved for use by agencies of the Department of Defense.

1. Scope*

1.1 These test methods cover the determination of flexural properties of unreinforced and reinforced plastics, including high-modulus composites and electrical insulating materials in the form of rectangular bars molded directly or cut from sheets, plates, or molded shapes. These test methods are generally applicable to both rigid and semirigid materials. However, flexural strength cannot be determined for those materials that do not break or that do not fail in the outer surface of the test specimen within the 5.0 % strain limit of these test methods. These test methods utilize a three-point loading system applied to a simply supported beam. A four-point loading system method can be found in Test Method D 6272.

1.1.1 *Procedure A*, designed principally for materials that break at comparatively small deflections.

1.1.2 *Procedure B*, designed particularly for those materials that undergo large deflections during testing.

1.1.3 Procedure A shall be used for measurement of flexural properties, particularly flexural modulus, unless the material specification states otherwise. Procedure B may be used for measurement of flexural strength only. Tangent modulus data obtained by Procedure A tends to exhibit lower standard deviations than comparable data obtained by means of Procedure B.

1.2 Comparative tests may be run in accordance with either procedure, provided that the procedure is found satisfactory for the material being tested.

1.3 The values stated in SI units are to be regarded as the standard. The values provided in parentheses are for information only.

1.4 *This standard does not purport to address all of the safety concerns, if any, associated with its use. It is the responsibility of the user of this standard to establish appropriate safety and health practices and determine the applicability of regulatory limitations prior to use.*

NOTE 1—These test methods are not technically equivalent to ISO 178.

2. Referenced Documents

2.1 *ASTM Standards:*

D 618 Practice for Conditioning Plastics for Testing[2]

D 638 Test Method for Tensile Properties of Plastics[2]

D 883 Terminology Relating to Plastics[2]

D 4000 Classification System for Specifying Plastic Materials[3]

D 5947 Test Methods for Physical Dimensions of Solid Plastic Specimens[4]

D 6272 Test Method for Flexural Properties of Unreinforced and Reinforced Plastics and Electrical Insulating Materials by Four-Point Bending[4]

E 4 Practices for Force Verification of Testing Machines[5]

E 691 Practice for Conducting an Interlaboratory Study to Determine the Precision of a Test Method[6]

3. Terminology

3.1 *Definitions*—Definitions of terms applying to these test methods appear in Terminology D 883 and Annex A1 of Test Method D 638.

4. Summary of Test Method

4.1 A bar of rectangular cross section rests on two supports and is loaded by means of a loading nose midway between the supports (see Fig. 1). A support span-to-depth ratio of 16:1 shall be used unless there is reason to suspect that a larger span-to-depth ratio may be required, as may be the case for certain laminated materials (see Section 7 and Note 8 for guidance).

4.2 The specimen is deflected until rupture occurs in the outer surface of the test specimen or until a maximum strain (see 12.7) of 5.0 % is reached, whichever occurs first.

4.3 Procedure A employs a strain rate of 0.01 mm/mm/min [0.01 in./in./min] and is the preferred procedure for this test method, while Procedure B employs a strain rate of 0.10 mm/mm/min [0.10 in./in./min].

[1] These test methods are under the jurisdiction of ASTM Committee D20 on Plastics and are the direct responsibility of Subcommittee D20.10 on Mechanical Properties.

Current edition approved March 10, 2003. Published April 2003. Originally approved in 1970. Last previous edition approved in 2002 as D 790 – 02.

[2] *Annual Book of ASTM Standards*, Vol 08.01.

[3] *Annual Book of ASTM Standards*, Vol 08.02.

[4] *Annual Book of ASTM Standards*, Vol 08.03.

[5] *Annual Book of ASTM Standards*, Vol 03.01.

[6] *Annual Book of ASTM Standards*, Vol 14.02.

*A Summary of Changes section appears at the end of this standard.

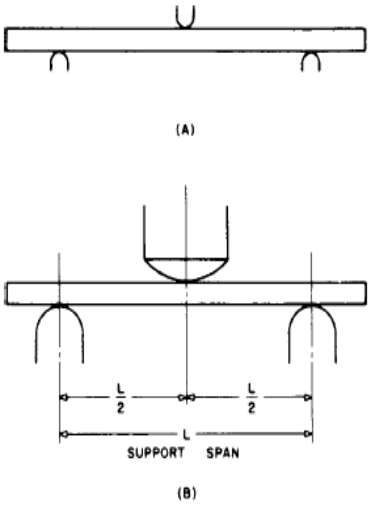

NOTE—(*a*) Minimum radius = 3.2 mm [⅛ in.]. (*b*) Maximum radius supports 1.6 times specimen depth; maximum radius loading nose = 4 times specimen depth.

FIG. 1 Allowable Range of Loading Nose and Support Radii

TABLE 1 Flexural Strength

Material	Mean, 10^3 psi	Values Expressed in Units of % of 10^3 psi			
		V_r[A]	V_R[B]	r[C]	R[D]
ABS	9.99	1.59	6.05	4.44	17.2
DAP thermoset	14.3	6.58	6.58	18.6	18.6
Cast acrylic	16.3	1.67	11.3	4.73	32.0
GR polyester	19.5	1.43	2.14	4.05	6.08
GR polycarbonate	21.0	5.16	6.05	14.6	17.1
SMC	26.0	4.76	7.19	13.5	20.4

[A] V_r = within-laboratory coefficient of variation for the indicated material. It is obtained by first pooling the within-laboratory standard deviations of the test results from all of the participating laboratories: $Sr = [[(s_1)^2 + (s_2)^2 \ldots + (s_n)^2]/n]^{1/2}$ then $V_r = (S_r$ divided by the overall average for the material) × 100.

[B] V_r = between-laboratory reproducibility, expressed as the coefficient of variation: $S_R = \{S_r^2 + S_L^2\}^{1/2}$ where S_L is the standard deviation of laboratory means. Then: $V_R = (S_R$ divided by the overall average for the material) × 100.

[C] r = within-laboratory critical interval between two test results = 2.8 × V_r.

[D] R = between-laboratory critical interval between two test results = 2.8 × V_R.

5. Significance and Use

5.1 Flexural properties as determined by these test methods are especially useful for quality control and specification purposes.

5.2 Materials that do not fail by the maximum strain allowed under these test methods (3-point bend) may be more suited to a 4-point bend test. The basic difference between the two test methods is in the location of the maximum bending moment and maximum axial fiber stresses. The maximum axial fiber stresses occur on a line under the loading nose in 3-point bending and over the area between the loading noses in 4-point bending.

5.3 Flexural properties may vary with specimen depth, temperature, atmospheric conditions, and the difference in rate of straining as specified in Procedures A and B (see also Note 8).

5.4 Before proceeding with these test methods, reference should be made to the specification of the material being tested. Any test specimen preparation, conditioning, dimensions, or testing parameters, or combination thereof, covered in the materials specification shall take precedence over those mentioned in these test methods. If there are no material specifications, then the default conditions apply. Table 1 in Classification System D 4000 lists the ASTM materials standards that currently exist for plastics.

6. Apparatus

6.1 *Testing Machine*— A properly calibrated testing machine that can be operated at constant rates of crosshead motion over the range indicated, and in which the error in the load measuring system shall not exceed ±1 % of the maximum load expected to be measured. It shall be equipped with a deflection measuring device. The stiffness of the testing machine shall be such that the total elastic deformation of the system does not exceed 1 % of the total deflection of the test specimen during testing, or appropriate corrections shall be made. The load indicating mechanism shall be essentially free from inertial lag at the crosshead rate used. The accuracy of the testing machine shall be verified in accordance with Practices E 4.

6.2 *Loading Noses and Supports*—The loading nose and supports shall have cylindrical surfaces. In order to avoid excessive indentation, or failure due to stress concentration directly under the loading nose, the radii of the loading nose and supports shall be 5.0 ± 0.1 mm [0.197 ± 0.004 in.] unless otherwise specified or agreed upon between the interested clients. When other loading noses and supports are used they must comply with the following requirements: they shall have a minimum radius of 3.2 mm [⅛ in.] for all specimens, and for specimens 3.2 mm or greater in depth, the radius of the supports may be up to 1.6 times the specimen depth. They shall be this large if significant indentation or compressive failure occurs. The arc of the loading nose in contact with the specimen shall be sufficiently large to prevent contact of the specimen with the sides of the nose (see Fig. 1). The maximum radius of the loading nose shall be no more than 4 times the specimen depth.

NOTE 2—Test data have shown that the loading nose and support dimensions can influence the flexural modulus and flexural strength values. The loading nose dimension has the greater influence. Dimensions of the loading nose and supports must be specified in the material specification.

6.3 *Micrometers*— Suitable micrometers for measuring the width and thickness of the test specimen to an incremental discrimination of at least 0.025 mm [0.001 in.] should be used. All width and thickness measurements of rigid and semirigid plastics may be measured with a hand micrometer with ratchet. A suitable instrument for measuring the thickness of nonrigid test specimens shall have: a contact measuring pressure of 25 ± 2.5 kPa [3.6 ± 0.36 psi], a movable circular contact foot 6.35 ± 0.025 mm [0.250 ± 0.001 in.] in diameter and a lower fixed anvil large enough to extend beyond the contact foot in all directions and being parallel to the contact foot within 0.005 mm [0.002 in.] over the entire foot area. Flatness of foot and anvil shall conform to the portion of the Calibration section of Test Methods D 5947.

7. Test Specimens

7.1 The specimens may be cut from sheets, plates, or molded shapes, or may be molded to the desired finished dimensions. The actual dimensions used in Section 4.2, Calculation, shall be measured in accordance with Test Methods D 5947.

NOTE 3—Any necessary polishing of specimens shall be done only in the lengthwise direction of the specimen.

7.2 *Sheet Materials (Except Laminated Thermosetting Materials and Certain Materials Used for Electrical Insulation, Including Vulcanized Fiber and Glass Bonded Mica)*:

7.2.1 *Materials 1.6 mm [1/16 in.] or Greater in Thickness*—For flatwise tests, the depth of the specimen shall be the thickness of the material. For edgewise tests, the width of the specimen shall be the thickness of the sheet, and the depth shall not exceed the width (see Notes 4 and 5). For all tests, the support span shall be 16 (tolerance ±1) times the depth of the beam. Specimen width shall not exceed one fourth of the support span for specimens greater than 3.2 mm [⅛ in.] in depth. Specimens 3.2 mm or less in depth shall be 12.7 mm [½ in.] in width. The specimen shall be long enough to allow for overhanging on each end of at least 10 % of the support span, but in no case less than 6.4 mm [¼ in.] on each end. Overhang shall be sufficient to prevent the specimen from slipping through the supports.

NOTE 4—Whenever possible, the original surface of the sheet shall be unaltered. However, where testing machine limitations make it impossible to follow the above criterion on the unaltered sheet, one or both surfaces shall be machined to provide the desired dimensions, and the location of the specimens with reference to the total depth shall be noted. The value obtained on specimens with machined surfaces may differ from those obtained on specimens with original surfaces. Consequently, any specifications for flexural properties on thicker sheets must state whether the original surfaces are to be retained or not. When only one surface was machined, it must be stated whether the machined surface was on the tension or compression side of the beam.

NOTE 5—Edgewise tests are not applicable for sheets that are so thin that specimens meeting these requirements cannot be cut. If specimen depth exceeds the width, buckling may occur.

7.2.2 *Materials Less than 1.6 mm [1/16 in.] in Thickness*—The specimen shall be 50.8 mm [2 in.] long by 12.7 mm [½ in.] wide, tested flatwise on a 25.4-mm [1-in.] support span.

NOTE 6—Use of the formulas for simple beams cited in these test methods for calculating results presumes that beam width is small in comparison with the support span. Therefore, the formulas do not apply rigorously to these dimensions.

NOTE 7—Where machine sensitivity is such that specimens of these dimensions cannot be measured, wider specimens or shorter support spans, or both, may be used, provided the support span-to-depth ratio is at least 14 to 1. All dimensions must be stated in the report (see also Note 6).

7.3 *Laminated Thermosetting Materials and Sheet and Plate Materials Used for Electrical Insulation, Including Vulcanized Fiber and Glass-Bonded Mica*—For paper-base and fabric-base grades over 25.4 mm [1 in.] in nominal thickness, the specimens shall be machined on both surfaces to a depth of 25.4 mm. For glass-base and nylon-base grades, specimens over 12.7 mm [½ in.] in nominal depth shall be machined on both surfaces to a depth of 12.7 mm. The support span-to-depth ratio shall be chosen such that failures occur in the outer fibers of the specimens, due only to the bending moment (see Note 8). Therefore, a ratio larger than 16:1 may be necessary (32:1 or 40:1 are recommended). When laminated materials exhibit low compressive strength perpendicular to the laminations, they shall be loaded with a large radius loading nose (up to four times the specimen depth to prevent premature damage to the outer fibers.

7.4 *Molding Materials (Thermoplastics and Thermosets)*—The recommended specimen for molding materials is 127 by 12.7 by 3.2 mm [5 by ½ by ⅛ in.] tested flatwise on a support span, resulting in a support span-to-depth ratio of 16 (tolerance ±1). Thicker specimens should be avoided if they exhibit significant shrink marks or bubbles when molded.

7.5 *High-Strength Reinforced Composites, Including Highly Orthotropic Laminates*—The span-to-depth ratio shall be chosen such that failure occurs in the outer fibers of the specimens and is due only to the bending moment (see Note 8). A span-to-depth ratio larger than 16:1 may be necessary (32:1 or 40:1 are recommended). For some highly anisotropic composites, shear deformation can significantly influence modulus measurements, even at span-to-depth ratios as high as 40:1. Hence, for these materials, an increase in the span-to-depth ratio to 60:1 is recommended to eliminate shear effects when modulus data are required, it should also be noted that the flexural modulus of highly anisotropic laminates is a strong function of ply-stacking sequence and will not necessarily correlate with tensile modulus, which is not stacking-sequence dependent.

NOTE 8—As a general rule, support span-to-depth ratios of 16:1 are satisfactory when the ratio of the tensile strength to shear strength is less than 8 to 1, but the support span-to-depth ratio must be increased for composite laminates having relatively low shear strength in the plane of the laminate and relatively high tensile strength parallel to the support span.

8. Number of Test Specimens

8.1 Test at least five specimens for each sample in the case of isotropic materials or molded specimens.

8.2 For each sample of anisotropic material in sheet form, test at least five specimens for each of the following conditions. Recommended conditions are flatwise and edgewise tests on specimens cut in lengthwise and crosswise directions of the sheet. For the purposes of this test, "lengthwise" designates the principal axis of anisotropy and shall be interpreted to mean the direction of the sheet known to be stronger in flexure. "Crosswise" indicates the sheet direction known to be the weaker in flexure and shall be at 90° to the lengthwise direction.

9. Conditioning

9.1 *Conditioning*—Condition the test specimens at 23 ± 2°C [73.4 ± 3.6°F] and 50 ± 5 % relative humidity for not less than 40 h prior to test in accordance with Procedure A of Practice D 618 unless otherwise specified by contract or the relevant ASTM material specification. Reference pre-test conditioning, to settle disagreements, shall apply tolerances of ±1°C [1.8°F] and ±2 % relative humidity.

9.2 *Test Conditions*—Conduct the tests at 23 ± 2°C [73.4 ± 3.6°F] and 50 ± 5 % relative humidity unless otherwise

specified by contract or the relevant ASTM material specification. Reference testing conditions, to settle disagreements, shall apply tolerances of ±1°C [1.8°F] and ±2 % relative humidity.

10. Procedure

10.1 *Procedure A*:

10.1.1 Use an untested specimen for each measurement. Measure the width and depth of the specimen to the nearest 0.03 mm [0.001 in.] at the center of the support span. For specimens less than 2.54 mm [0.100 in.] in depth, measure the depth to the nearest 0.003 mm [0.0005 in.]. These measurements shall be made in accordance with Test Methods D 5947.

10.1.2 Determine the support span to be used as described in Section 7 and set the support span to within 1 % of the determined value.

10.1.3 For flexural fixtures that have continuously adjustable spans, measure the span accurately to the nearest 0.1 mm [0.004 in.] for spans less than 63 mm [2.5 in.] and to the nearest 0.3 mm [0.012 in.] for spans greater than or equal to 63 mm [2.5 in.]. Use the actual measured span for all calculations. For flexural fixtures that have fixed machined span positions, verify the span distance the same as for adjustable spans at each machined position. This distance becomes the span for that position and is used for calculations applicable to all subsequent tests conducted at that position. See Annex A2 for information on the determination of and setting of the span.

10.1.4 Calculate the rate of crosshead motion as follows and set the machine for the rate of crosshead motion as calculated by Eq 1:

$$R = ZL^2/6d \quad (1)$$

where:

R = rate of crosshead motion, mm [in.]/min,
L = support span, mm [in.],
d = depth of beam, mm [in.], and
Z = rate of straining of the outer fiber, mm/mm/min [in./in./min]. Z shall be equal to 0.01.

In no case shall the actual crosshead rate differ from that calculated using Eq 1, by more than ±10 %.

10.1.5 Align the loading nose and supports so that the axes of the cylindrical surfaces are parallel and the loading nose is midway between the supports. The parallelism of the apparatus may be checked by means of a plate with parallel grooves into which the loading nose and supports will fit when properly aligned (see A2.3). Center the specimen on the supports, with the long axis of the specimen perpendicular to the loading nose and supports.

10.1.6 Apply the load to the specimen at the specified crosshead rate, and take simultaneous load-deflection data. Measure deflection either by a gage under the specimen in contact with it at the center of the support span, the gage being mounted stationary relative to the specimen supports, or by measurement of the motion of the loading nose relative to the supports. Load-deflection curves may be plotted to determine the flexural strength, chord or secant modulus or the tangent modulus of elasticity, and the total work as measured by the area under the load-deflection curve. Perform the necessary toe compensation (see Annex A1) to correct for seating and indentation of the specimen and deflections in the machine.

10.1.7 Terminate the test when the maximum strain in the outer surface of the test specimen has reached 0.05 mm/mm [in./in.] or at break if break occurs prior to reaching the maximum strain (Notes 9 and 10). The deflection at which this strain will occur may be calculated by letting r equal 0.05 mm/mm [in./in.] in Eq 2:

$$D = rL^2/6d \quad (2)$$

where:

D = midspan deflection, mm [in.],
r = strain, mm/mm [in./in.],
L = support span, mm [in.], and
d = depth of beam, mm [in.].

NOTE 9—For some materials that do not yield or break within the 5 % strain limit when tested by Procedure A, the increased strain rate allowed by Procedure B (see 10.2) may induce the specimen to yield or break, or both, within the required 5 % strain limit.

NOTE 10—Beyond 5 % strain, this test method is not applicable. Some other mechanical property might be more relevant to characterize materials that neither yield nor break by either Procedure A or Procedure B within the 5 % strain limit (for example, Test Method D 638 may be considered).

10.2 *Procedure B*:

10.2.1 Use an untested specimen for each measurement.

10.2.2 Test conditions shall be identical to those described in 10.1, except that the rate of straining of the outer surface of the test specimen shall be 0.10 mm/mm [in./in.]/min.

10.2.3 If no break has occurred in the specimen by the time the maximum strain in the outer surface of the test specimen has reached 0.05 mm/mm [in./in.], discontinue the test (see Note 10).

11. Retests

11.1 Values for properties at rupture shall not be calculated for any specimen that breaks at some obvious, fortuitous flaw, unless such flaws constitute a variable being studied. Retests shall be made for any specimen on which values are not calculated.

12. Calculation

12.1 Toe compensation shall be made in accordance with Annex A1 unless it can be shown that the toe region of the curve is not due to the take-up of slack, seating of the specimen, or other artifact, but rather is an authentic material response.

12.2 *Flexural Stress* (σ_f)—When a homogeneous elastic material is tested in flexure as a simple beam supported at two points and loaded at the midpoint, the maximum stress in the outer surface of the test specimen occurs at the midpoint. This stress may be calculated for any point on the load-deflection curve by means of the following equation (see Notes 11-13):

$$\sigma_f = 3PL/2bd^2 \quad (3)$$

where:

σ = stress in the outer fibers at midpoint, MPa [psi],

P = load at a given point on the load-deflection curve, N [lbf],
L = support span, mm [in.],
b = width of beam tested, mm [in.], and
d = depth of beam tested, mm [in.].

NOTE 11—Eq 3 applies strictly to materials for which stress is linearly proportional to strain up to the point of rupture and for which the strains are small. Since this is not always the case, a slight error will be introduced if Eq 3 is used to calculate stress for materials that are not true Hookean materials. The equation is valid for obtaining comparison data and for specification purposes, but only up to a maximum fiber strain of 5 % in the outer surface of the test specimen for specimens tested by the procedures described herein.

NOTE 12—When testing highly orthotropic laminates, the maximum stress may not always occur in the outer surface of the test specimen.[7] Laminated beam theory must be applied to determine the maximum tensile stress at failure. If Eq 3 is used to calculate stress, it will yield an apparent strength based on homogeneous beam theory. This apparent strength is highly dependent on the ply-stacking sequence of highly orthotropic laminates.

NOTE 13—The preceding calculation is not valid if the specimen slips excessively between the supports.

12.3 *Flexural Stress for Beams Tested at Large Support Spans (σ_f)*—If support span-to-depth ratios greater than 16 to 1 are used such that deflections in excess of 10 % of the support span occur, the stress in the outer surface of the specimen for a simple beam can be reasonably approximated with the following equation (see Note 14):

$$\sigma_f = (3PL/2bd^2)[1 + 6(D/L)^2 - 4(d/L)(D/L)] \quad (4)$$

where:

σ_f, P, L, b, and d are the same as for Eq 3, and
D = deflection of the centerline of the specimen at the middle of the support span, mm [in.].

NOTE 14—When large support span-to-depth ratios are used, significant end forces are developed at the support noses which will affect the moment in a simple supported beam. Eq 4 includes additional terms that are an approximate correction factor for the influence of these end forces in large support span-to-depth ratio beams where relatively large deflections exist.

12.4 *Flexural Strength (σ_{fM})*—Maximum flexural stress sustained by the test specimen (see Note 12) during a bending test. It is calculated according to Eq 3 or Eq 4. Some materials that do not break at strains of up to 5 % may give a load deflection curve that shows a point at which the load does not increase with an increase in strain, that is, a yield point (Fig. 2, Curve B), *Y*. The flexural strength may be calculated for these materials by letting P (in Eq 3 or Eq 4) equal this point, *Y*.

12.5 *Flexural Offset Yield Strength*—Offset yield strength is the stress at which the stress-strain curve deviates by a given strain (offset) from the tangent to the initial straight line portion of the stress-strain curve. The value of the offset must be given whenever this property is calculated.

NOTE 15—This value may differ from flexural strength defined in 12.4.

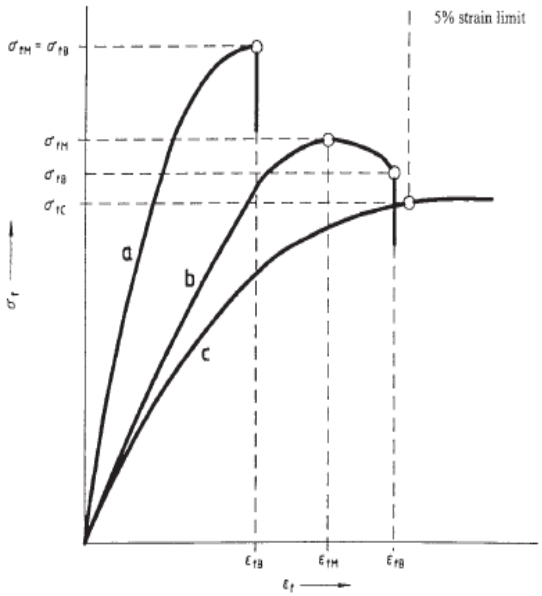

NOTE—Curve a: Specimen that breaks before yielding.
Curve b: Specimen that yields and then breaks before the 5 % strain limit.
Curve c: Specimen that neither yields nor breaks before the 5 % strain limit.

FIG. 2 Typical Curves of Flexural Stress (s_f) Versus Flexural Strain (ϵ_f)

Both methods of calculation are described in the annex to Test Method D 638.

12.6 *Flexural Stress at Break (σ_{fB})*—Flexural stress at break of the test specimen during a bending test. It is calculated according to Eq 3 or Eq 4. Some materials may give a load deflection curve that shows a break point, *B*, without a yield point (Fig. 2, Curve a) in which case $\sigma_{fB} = \sigma_{fM}$. Other materials may give a yield deflection curve with both a yield and a break point, *B* (Fig. 2, Curve b). The flexural stress at break may be calculated for these materials by letting P (in Eq 3 or Eq 4) equal this point, *B*.

12.7 *Stress at a Given Strain*—The stress in the outer surface of a test specimen at a given strain may be calculated in accordance with Eq 3 or Eq 4 by letting P equal the load read from the load-deflection curve at the deflection corresponding to the desired strain (for highly orthotropic laminates, see Note 12).

12.8 *Flexural Strain, ϵ_f*—Nominal fractional change in the length of an element of the outer surface of the test specimen at midspan, where the maximum strain occurs. It may be calculated for any deflection using Eq 5:

$$\epsilon_f = 6Dd/L^2 \quad (5)$$

where:

ϵ_f = strain in the outer surface, mm/mm [in./in.],
D = maximum deflection of the center of the beam, mm [in.],
L = support span, mm [in.], and

[7] For a discussion of these effects, see Zweben, C., Smith, W. S., and Wardle, M. W., "Test Methods for Fiber Tensile Strength, Composite Flexural Modulus and Properties of Fabric-Reinforced Laminates, " *Composite Materials: Testing and Design (Fifth Conference), ASTM STP 674*, 1979, pp. 228–262.

d = depth, mm [in.].
D = maximum deflection of the center of the beam, mm [in.],
L = support span, mm [in.], and
d = depth, mm [in.].

12.9 *Modulus of Elasticity*:

12.9.1 *Tangent Modulus of Elasticity*—The tangent modulus of elasticity, often called the "modulus of elasticity," is the ratio, within the elastic limit, of stress to corresponding strain. It is calculated by drawing a tangent to the steepest initial straight-line portion of the load-deflection curve and using Eq 6 (for highly anisotropic composites, see Note 16).

$$E_B = L^3m/4bd^3 \quad (6)$$

where:
E_B = modulus of elasticity in bending, MPa [psi],
L = support span, mm [in.],
b = width of beam tested, mm [in.],
d = depth of beam tested, mm [in.], and
m = slope of the tangent to the initial straight-line portion of the load-deflection curve, N/mm [lbf/in.] of deflection.

NOTE 16—Shear deflections can seriously reduce the apparent modulus of highly anisotropic composites when they are tested at low span-to-depth ratios.[7] For this reason, a span-to-depth ratio of 60 to 1 is recommended for flexural modulus determinations on these composites. Flexural strength should be determined on a separate set of replicate specimens at a lower span-to-depth ratio that induces tensile failure in the outer fibers of the beam along its lower face. Since the flexural modulus of highly anisotropic laminates is a critical function of ply-stacking sequence, it will not necessarily correlate with tensile modulus, which is not stacking-sequence dependent.

12.9.2 *Secant Modulus*— The secant modulus is the ratio of stress to corresponding strain at any selected point on the stress-strain curve, that is, the slope of the straight line that joins the origin and a selected point on the actual stress-strain curve. It shall be expressed in megapascals [pounds per square inch]. The selected point is chosen at a prespecified stress or strain in accordance with the appropriate material specification or by customer contract. It is calculated in accordance with Eq 6 by letting m equal the slope of the secant to the load-deflection curve. The chosen stress or strain point used for the determination of the secant shall be reported.

12.9.3 *Chord Modulus (E_f)*—The chord modulus may be calculated from two discrete points on the load deflection curve. The selected points are to be chosen at two prespecified stress or strain points in accordance with the appropriate material specification or by customer contract. The chosen stress or strain points used for the determination of the chord modulus shall be reported. Calculate the chord modulus, E_f using the following equation:

$$E_f = (\sigma_{f2} - \sigma_{f1})/(\epsilon_{f2} - \epsilon_{f1}) \quad (7)$$

where:

σ_{f2} and σ_{f1} are the flexural stresses, calculated from Eq 3 or Eq 4 and measured at the predefined points on the load deflection curve, and ϵ_{f2} and

ϵ_{f1} are the flexural strain values, calculated from Eq 5 and measured at the predetermined points on the load deflection curve.

12.10 *Arithmetic Mean*— For each series of tests, the arithmetic mean of all values obtained shall be calculated to three significant figures and reported as the "average value" for the particular property in question.

12.11 *Standard Deviation*—The standard deviation (estimated) shall be calculated as follows and be reported to two significant figures:

$$s = \sqrt{(\Sigma X^2 - n\bar{X}^2)/(n-1)} \quad (8)$$

where:
s = estimated standard deviation,
X = value of single observation,
n = number of observations, and
$\bar{X}$ = arithmetic mean of the set of observations.

TABLE 2 Flexural Modulus

Material	Mean, 10^3 psi	Values Expressed in units of % of 10^3 psi			
		V_r[A]	V_R[B]	r[C]	R[D]
ABS	338	4.79	7.69	13.6	21.8
DAP thermoset	485	2.89	7.18	8.15	20.4
Cast acrylic	810	13.7	16.1	38.8	45.4
GR polyester	816	3.49	4.20	9.91	11.9
GR polycarbonate	1790	5.52	5.52	15.6	15.6
SMC	1950	10.9	13.8	30.8	39.1

[A] V_r = within-laboratory coefficient of variation for the indicated material. It is obtained by first pooling the within-laboratory standard deviations of the test results from all of the participating laboratories: $Sr = [[(s_1)^2 + (s_2)^2 \ldots + (s_n)^2]/n]^{1/2}$ then V_r = (S_r divided by the overall average for the material) × 100.
[B] V_r = between-laboratory reproducibility, expressed as the coefficient of variation: $S_R = \{S_r^2 + S_L^2\}^{1/2}$ where S_L is the standard deviation of laboratory means. Then: V_R = (S_R divided by the overall average for the material) × 100.
[C] r = within-laboratory critical interval between two test results = 2.8 × V_r.
[D] R = between-laboratory critical interval between two test results = 2.8 × V_R.

13. Report

13.1 Report the following information:

13.1.1 Complete identification of the material tested, including type, source, manufacturer's code number, form, principal dimensions, and previous history (for laminated materials, ply-stacking sequence shall be reported),

13.1.2 Direction of cutting and loading specimens, when appropriate,

13.1.3 Conditioning procedure,

13.1.4 Depth and width of specimen,

13.1.5 Procedure used (A or B),

13.1.6 Support span length,

13.1.7 Support span-to-depth ratio if different than 16:1,

13.1.8 Radius of supports and loading noses if different than 5 mm,

13.1.9 Rate of crosshead motion,

13.1.10 Flexural strain at any given stress, average value and standard deviation,

13.1.11 If a specimen is rejected, reason(s) for rejection,

13.1.12 Tangent, secant, or chord modulus in bending, average value, standard deviation, and the strain level(s) used if secant or chord modulus,

13.1.13 Flexural strength (if desired), average value, and standard deviation,

13.1.14 Stress at any given strain up to and including 5 % (if desired), with strain used, average value, and standard deviation,

13.1.15 Flexural stress at break (if desired), average value, and standard deviation,

13.1.16 Type of behavior, whether yielding or rupture, or both, or other observations, occurring within the 5 % strain limit, and

13.1.17 Date of specific version of test used.

14. Precision and Bias [8]

14.1 Tables 1 and 2 are based on a round-robin test conducted in 1984, in accordance with Practice E 691, involving six materials tested by six laboratories using Procedure A. For each material, all the specimens were prepared at one source. Each "test result" was the average of five individual determinations. Each laboratory obtained two test results for each material.

NOTE 17—**Caution:** The following explanations of *r* and *R* (14.2-14.2.3) are intended only to present a meaningful way of considering the approximate precision of these test methods. The data given in Tables 2 and 3 should not be applied rigorously to the acceptance or rejection of materials, as those data are specific to the round robin and may not be representative of other lots, conditions, materials, or laboratories. Users of these test methods should apply the principles outlined in Practice E 691 to generate data specific to their laboratory and materials, or between specific laboratories. The principles of 14.2-14.2.3 would then be valid for such data.

14.2 *Concept of "r" and "R" in* Tables 1 and 2—If S_r and S_R have been calculated from a large enough body of data, and for test results that were averages from testing five specimens for each test result, then:

14.2.1 *Repeatability*— Two test results obtained within one laboratory shall be judged not equivalent if they differ by more than the *r* value for that material. *r* is the interval representing the critical difference between two test results for the same material, obtained by the same operator using the same equipment on the same day in the same laboratory.

14.2.2 *Reproducibility*— Two test results obtained by different laboratories shall be judged not equivalent if they differ by more than the *R* value for that material. *R* is the interval representing the critical difference between two test results for the same material, obtained by different operators using different equipment in different laboratories.

14.2.3 The judgments in 14.2.1 and 14.2.2 will have an approximately 95 % (0.95) probability of being correct.

14.3 *Bias*—No statement may be made about the bias of these test methods, as there is no standard reference material or reference test method that is applicable.

15. Keywords

15.1 flexural properties; plastics; stiffness; strength

[8] Supporting data are available from ASTM Headquarters. Request RR: D20 – 1128.

ANNEXES

(Mandatory Information)

A1. TOE COMPENSATION

A1.1 In a typical stress-strain curve (see Fig. A1.1) there is a toe region, *AC,* that does not represent a property of the material. It is an artifact caused by a takeup of slack and alignment or seating of the specimen. In order to obtain correct values of such parameters as modulus, strain, and offset yield point, this artifact must be compensated for to give the corrected zero point on the strain or extension axis.

A1.2 In the case of a material exhibiting a region of Hookean (linear) behavior (see Fig. A1.1), a continuation of the linear *(CD)* region of the curve is constructed through the zero-stress axis. This intersection *(B)* is the corrected zero-strain point from which all extensions or strains must be measured, including the yield offset *(BE),* if applicable. The elastic modulus can be determined by dividing the stress at any point along the Line *CD* (or its extension) by the strain at the same point (measured from Point *B,* defined as zero-strain).

A1.3 In the case of a material that does not exhibit any linear region (see Fig. A1.2), the same kind of toe correction of the zero-strain point can be made by constructing a tangent to the maximum slope at the inflection Point *H′*. This is extended to intersect the strain axis at Point *B′*, the corrected zero-strain

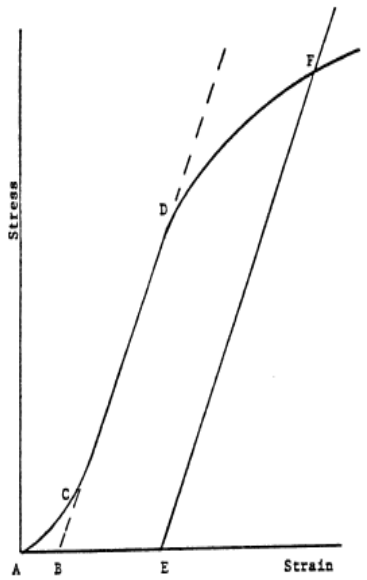

NOTE—Some chart recorders plot the mirror image of this graph.

FIG. A1.1 Material with Hookean Region

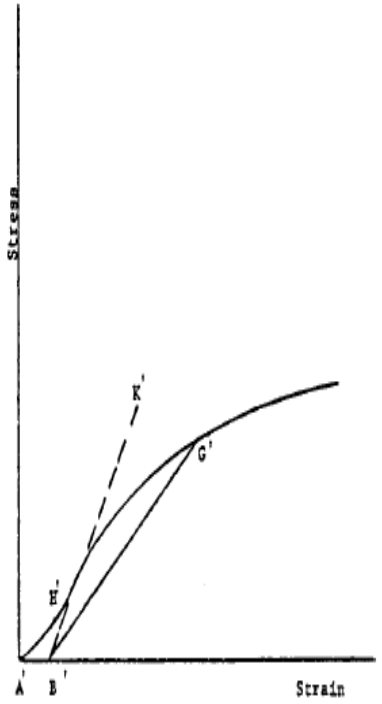

NOTE—Some chart recorders plot the mirror image of this graph.

FIG. A1.2 Material with No Hookean Region

point. Using Point B' as zero strain, the stress at any point (G') on the curve can be divided by the strain at that point to obtain a secant modulus (slope of Line B' G'). For those materials with no linear region, any attempt to use the tangent through the inflection point as a basis for determination of an offset yield point may result in unacceptable error.

A2. MEASURING AND SETTING SPAN

A2.1 For flexural fixtures that have adjustable spans, it is important that the span between the supports is maintained constant or the actual measured span is used in the calculation of stress, modulus, and strain, and the loading nose or noses are positioned and aligned properly with respect to the supports. Some simple steps as follows can improve the repeatability of your results when using these adjustable span fixtures.

A2.2 Measurement of Span:

A2.2.1 This technique is needed to ensure that the correct span, not an estimated span, is used in the calculation of results.

A2.2.2 Scribe a permanent line or mark at the exact center of the support where the specimen makes complete contact. The type of mark depends on whether the supports are fixed or rotatable (see Figs. A2.1 and A2.2).

A2.2.3 Using a vernier caliper with pointed tips that is readable to at least 0.1 mm [0.004 in.], measure the distance between the supports, and use this measurement of span in the calculations.

FIG. A2.1 Markings on Fixed Specimen Supports

FIG. A2.2 Markings on Rotatable Specimen Supports

A2.3 *Setting the Span and Alignment of Loading Nose(s)*—To ensure a consistent day-to-day setup of the span and ensure the alignment and proper positioning of the loading nose, simple jigs should be manufactured for each of the standard setups used. An example of a jig found to be useful is shown in Fig. A2.3.

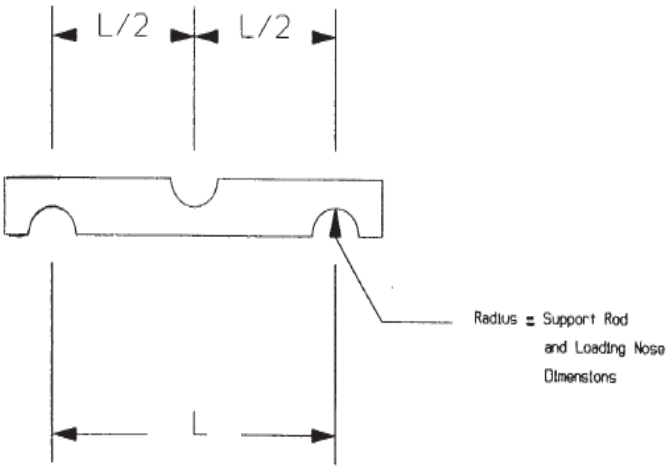

FIG. A2.3 Fixture Used to Set Loading Nose and Support Spacing and Alignment

APPENDIX

(Nonmandatory Information)

X1. DEVELOPMENT OF A FLEXURAL MACHINE COMPLIANCE CORRECTION

X1.1 Introduction

X1.1.1 Universal Testing instrument drive systems always exhibit a certain level of compliance that is characterized by a variance between the reported crosshead displacement and the displacement actually imparted to the specimen. This variance is a function of load frame stiffness, drive system wind-up, load cell compliance and fixture compliance. To accurately measure the flexural modulus of a material, this compliance should be measured and empirically subtracted from test data. Flexural modulus results without the corrections are lower than if the correction is applied. The greater the stiffness of the material the more influence the system compliance has on results.

X1.1.2 It is not necessary to make the machine compliance correction when a deflectometer/extensometer is used to measure the actual deflection occurring in the specimen as it is deflected.

X1.2 Terminology

X1.2.1 *Compliance*—The displacement difference between test machine drive system displacement values and actual specimen displacement

X1.2.2 *Compliance Correction*—An analytical method of modifying test instrument displacement values to eliminate the amount of that measurement attributed to test instrument compliance.

X1.3 Apparatus

X1.3.1 Universal Testing machine

X1.3.2 Load cell

X1.3.3 Flexure fixture including loading nose and specimen supports

X1.3.4 Computer Software to make corrections to the displacements

X1.3.5 Steel bar, with smoothed surfaces and a calculated flexural stiffness of more than 100 times greater than the test material. The length should be at least 13 mm greater than the support span. The width shall match the width of the test specimen and the thickness shall be that required to achieve or exceed the target stiffness.

X1.4 Safety Precautions

X1.4.1 The universal testing machine should stop the machine crosshead movement when the load reaches 90 % of load cell capacity, to prevent damage to the load cell.

X1.4.2 The compliance curve determination should be made at a speed no higher than 2 mm/min. Because the load builds up rapidly since the steel bar does not deflect, it is quite easy to exceed the load cell capacity.

X1.5 Procedure

NOTE X1.1—A new compliance correction curve should be established each time there is a change made to the setup of the test machine, such as, load cell changed or reinstallation of the flexure fixture on the machine. If the test machine is dedicated to flexural testing, and there are no changes to the setup, it is not necessary to re-calculate the compliance curve.

NOTE X1.2—On those machines with computer software that automatically make this compliance correction; refer to the software manual to determine how this correction should be made.

X1.5.1 The procedure to determine compliance follows:

X1.5.1.1 Configure the test system to match the actual test configuration.

X1.5.1.2 Place the steel bar in the test fixture, duplicating the position of a specimen during actual testing.

X1.5.1.3 Set the crosshead speed to 2 mm/min. or less and start the crosshead moving in the test direction recording crosshead displacement and the corresponding load values.

X1.5.1.4 Increase load to a point exceeding the highest load expected during specimen testing. Stop the crosshead and return to the pre-test location.

X1.5.1.5 The recorded load-deflection curve, starting when the loading nose contacts the steel bar to the time that the highest load expected is defined as test system compliance.

X1.5.2 Procedure to apply compliance correction is as follows:

X1.5.2.1 Run the flexural test method on the material at the crosshead required for the measurement.

X1.5.2.2 It is preferable that computer software be used to make the displacement corrections, but if it is not available compliance corrections can be made manually in the following manner. Determine the range of displacement (D) on the load versus displacement curve for the material, over which the modulus is to be calculated. For Young's Modulus that would steepest region of the curve below the proportional limit. For Secant and Chord Modulii that would be at specified level of strain or specified levels of strain, respectively. Draw two vertical lines up from the displacement axis for the two chosen displacements (D1, D2) to the load versus displacement curve for the material. In some cases one of these points maybe at zero displacement after the toe compensation correction is made. Draw two horizontal lines from these points on the load displacement curve to the Load (P) axis. Determine the loads (L1, L2).

X1.5.2.3 Using the Compliance Correction load displacement curve for the steel bar, mark off L1 and L2 on the Load (P) axis. From these two points draw horizontal lines across till they contact the load versus displacement curve for the steel bar. From these two points on the load deflection curve draw two vertical lines downwards to the displacement axis. These two points on the displacement axis determine the corrections (c1, c2) that need to be made to the displacements measurements for the test material.

X1.5.2.4 Subtract the corrections (c1, c2) from the measured displacements (D1, D2), so that a true measures of test specimen deflection (D1-c1, D2-c2) are obtained.

X1.6 Calculations

X1.6.1 Calculation of Chord Modulus

X1.6.1.1 Calculate the stresses ($\sigma f1$, $\sigma f2$) for load points L1 and L2 from Fig. X1.1 using the equation in 12.2 3.

X1.6.1.2 Calculate the strains ($\epsilon f1$, $\epsilon f2$) for displacements D1-c1 and D2-c2 from Fig. X1.3 using the equation in 12.8 Eq. 5.

X1.6.1.3 Calculate the flexural chord modulus in accordance with 12.9.3 Eq. 7.

X1.6.2 Calculation of Secant Modulus

X1.6.2.1 Calculation of the Secant Modulus at any strain along the curve would be the same as conducting a chord modulus measurement, except that $\sigma f1 = 0$, L1= 0, and D1-c1 = 0.

X1.6.3 Calculation of Young's Modulus

X1.6.3.1 Determine the steepest slope "m" along the curve, below the proportional limit, using the selected loads L1 and L2 from Fig. X1.1 and the displacements D1-c1 and D2-c2 from Fig. X1.3.

X1.6.3.2 Calculate the Young's modulus in accordance with 12.9.1 Eq. 6.

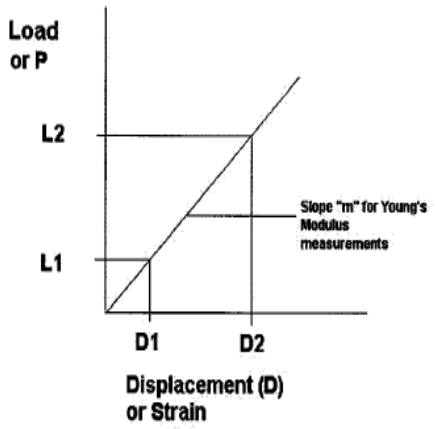

FIG. X1.1 Example of Modulus Curve for a Material

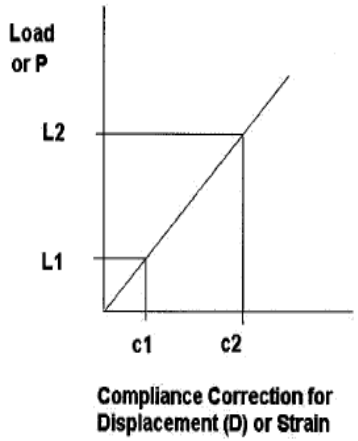

FIG. X1.2 Compliance Curve for Steel Bar

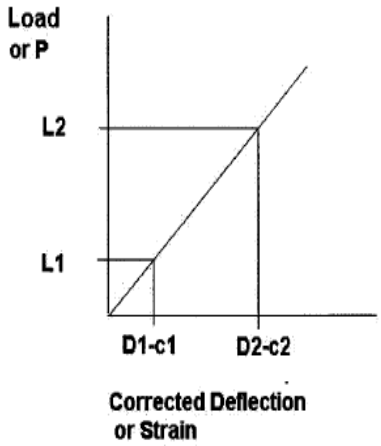

FIG. X1.3 Example of the Material Curve Corrected for the Compliance Corrected Displacement or Strain

SUMMARY OF CHANGES

This section identifies the location of selected changes to these test methods. For the convenience of the user, Committee D20 has highlighted those changes that may impact the use of these test methods. This section may also include descriptions of the changes or reasons for the changes, or both.

D 790 – 03:

(*1*) Added Appendix X1.

D 790 – 02:

(*1*) Revised 9.1 and 9.2.

D 790 – 00:

(*1*) Revised 12.1.

D 790 – 99:

(*1*) Revised 10.1.3.

D 790 – 98:

(*1*) Section 4.2 was rewritten extensively to bring this standard closer to ISO 178.

(*2*) Fig. 2 was added to clarify flexural behaviors that may be observed and to define what yielding and breaking behaviors look like, as well as the appropriate place to select these points on the stress strain curve.